Developmental Biology
Genetics and Genomics

Inhibitory G proteins play multiple roles to polarize sensory hair cell morphogenesis

Reviewed Preprint

Revised by authors after peer review.

About eLife's process

Reviewed preprint version 2
April 4, 2024 (this version)

Reviewed preprint version 1
July 18, 2023

Posted to preprint server
May 25, 2023

Sent for peer review
May 2, 2023

Amandine Jarysta, Abigail L.D. Tadenev, Matthew Day, Barry Krawchuk, Benjamin E. Low, Michael V. Wiles, Basile Tarchini

The Jackson Laboratory, Bar Harbor, ME 04609, USA. • Tufts University School of Medicine, Boston, MA 02111, USA

Abstract

Inhibitory G alpha (GNAI or Gαi) proteins are critical for the polarized morphogenesis of sensory hair cells and for hearing. The extent and nature of their actual contributions remains unclear, however, as previous studies did not investigate all GNAI proteins and included non-physiological approaches. Pertussis toxin can downregulate functionally redundant GNAI1, GNAI2, GNAI3 and GNAO proteins, but may also induce unrelated defects. Here we directly and systematically determine the role(s) of each individual GNAI protein in mouse auditory hair cells. GNAI2 and GNAI3 are similarly polarized at the hair cell apex with their binding partner GPSM2, whereas GNAI1 and GNAO are not detected. In *Gnai3* mutants, GNAI2 progressively fails to fully occupy the subcellular compartments where GNAI3 is missing. In contrast, GNAI3 can fully compensate for the loss of GNAI2 and is essential for hair bundle morphogenesis and auditory function. Simultaneous inactivation of *Gnai2* and *Gnai3* recapitulates for the first time two distinct types of defects only observed so far with pertussis toxin: 1) a delay or failure of the basal body to migrate off-center in prospective hair cells, and 2) a reversal in the orientation of some hair cell types. We conclude that GNAI proteins are critical for hair cells to break planar symmetry and to orient properly before GNAI2/3 regulate hair bundle morphogenesis with GPSM2.

eLife assessment

This study examines an **important** aspect of the development of the auditory system, the role of guanine nucleotide-binding protein subunits, GNAIs, in stereociliary bundle formation and orientation, by examining bundle phenotypes in multiple compound GNAI mutants. The experiments are highly rigorous and thorough and include detailed quantifications of bundle morphologies and changes. The depth and care of the study are impressive, with **convincing** results regarding the roles of GNAIs in stereociliary bundle development. Further, the reviewers believe this to be the definitive study of the role of GNAIs in bundle orientation and development.

Introduction

Developing sensory hair cells (HC) in the inner ear undergo a complex polarization process to detect and interpret mechanical stimuli, including sound. Each mature HC is able to detect stimuli in a directional manner by developing an asymmetric brush of actin-based membrane protrusions, or stereocilia: the hair bundle. Neighboring HC also adopt concerted orientations to align their hair bundles, a property known as planar cell polarity (PCP). One subclass of heterotrimeric guanine nucleotide-binding (G) protein was intimately associated with different levels of mouse HC polarization: inhibitory G alpha subunits (GNAI1, GNAI2, GNAI3 and GNAO; collectively GNAI or Gχξi) (**Figure 1A**). However, several roles proposed for GNAI proteins have not been validated physiologically, and the individual contribution of each GNAI remains uncertain.

HC polarization along the epithelial plane starts with the off-center migration of the basal body and its associated primary cilium, the kinocilium (Denman-Johnson & Forge, 1999; Mbiene & Sans, 1986; Tilney et al, 1992). At that stage, Regulator of G protein Signaling 12 (RGS12) is required for GNAI and the G protein signaling modulator 2 (GPSM2) scaffold to form a polarized complex at the apical membrane on the side of the off-center basal body (Akturk et al, 2022; Ezan et al, 2013; Tarchini et al, 2013). GPSM2-GNAI is best known as a highly conserved protein complex orienting the mitotic spindle during progenitor divisions (Du et al, 2001; Schaefer et al, 2001; Schaefer et al, 2000; Woodard et al, 2010). In post-mitotic HC, GPSM2-GNAI first excludes microvilli and microvilli-derived stereocilia from the portion of the HC surface where it resides, the expanding bare zone (**Figure 1B**). Bare zone expansion then pushes back the basal body/kinocilium from a more eccentric position near the lateral junction to a less eccentric position at the vertex of the forming hair bundle. Later, GPSM2-GNAI becomes enriched at the distal tip of row 1 stereocilia abutting the bare zone (Tarchini et al, 2016). In these stereocilia, GPSM2-GNAI is a module of the elongation complex that also comprises MYO15A, WHRN and EPS8 (Mauriac et al, 2017; Tadenev et al, 2019). GPSM2-GNAI is required at row 1 tips for boosting enrichment of other elongation complex partners, and presumably actin incorporation, compared to further stereocilia rows. GPSM2-GNAI thus confers row 1 its tallest identity and the hair bundle its asymmetric graded-height morphology.

Pertussis toxin (ptx) has been extensively used as a tool to ADP-ribosylate the GNAI subunit and dissociate heterotrimeric Gαiγγ protein complexes from G protein-coupled receptors (GPCR) to inactivate downstream signaling (Locht et al, 2011). *In vivo* expression of ptx catalytic subunit (ptx-S1 or ptxA) prevents normal enrichment and polarization of GPSM2-GNAI in developing HC (Tadenev et al, 2019; Tarchini et al, 2013), suggesting that ADP-ribosylation directly or indirectly inhibits GPSM2-GNAI function as well. Ptx provokes immature-looking hair bundles with severely stunted stereocilia, mimicking defects in *Gpsm2* mutants and *Gnai2; Gnai3* double mutants (Beer-Hammer et al, 2018; Mauriac et al, 2017; Tadenev et al, 2019; Tarchini et al, 2016). In contrast, stereocilia height is more variably reduced in *Gnai3* single mutants, with defects more severe at the cochlear base (Beer-Hammer et al, 2018; Mauriac et al, 2017). This can explain why hearing loss is more severe at high frequencies in *Gnai3* mutants, but profound at all frequencies in a *ptxA* model and in mutants lacking GPSM2 or both GNAI2 and GNAI3 (Beer-Hammer et al, 2018; Mauriac et al, 2017; Tarchini et al, 2016). Surprisingly, before affecting hair bundle differentiation at postnatal stages, ptx also causes two distinct defects in HC polarization at embryonic stages.

First, one study reported that a high dose of ptx in cultured explants of the developing cochlea results in a low proportion of symmetrical HC with a central kinocilium surrounded by a rounded hair bundle (**Figure 1C**) (Ezan et al, 2013). Because GPSM2-GNAI recruits partners to pull on astral microtubules during mitotic spindle orientation, the authors proposed that GPSM2-GNAI

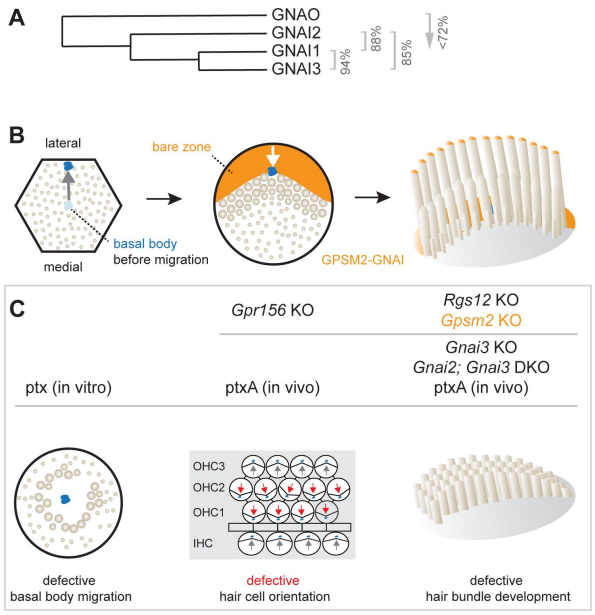

Figure 1.

Summary of GNAI-related functions proposed previously in hair cells.

A) Phylogenetic tree of GNAI/O proteins with percent amino acid identity (mouse). **B)** Apical HC differentiation from symmetry breaking to hair bundle development. The distribution of the GPSM2-GNAI complex at the bare zone and stereocilia tips is indicated in orange. Arrows indicate off-center (left) and then inward (middle) movements of the basal body. **C)** Defects observed with pertussis toxin (ptx) or when inactivating GNAI proteins. Defective off-center migration of the basal body and inverted OHC1-2 were only observed with ptx, respectively in cochlear explants (in vitro) and by expressing the ptx catalytic subunit (ptxA) in vivo. Mouse knock-out (KO)s of *Gnai* genes were to date only reported to affect hair bundle morphogenesis. Known GNAI regulators that produce similar defects when inactivated are indicated on top for each type of defect. DKO, double KO.

functions similarly and triggers the basal body off-center migration when post-mitotic HC break planar symmetry. However, this hypothesis has not been validated *in vivo* to date. Studies where *Gpsm2* (Bhonker et al, 2016; Ezan et al, 2013; Mauriac et al, 2017; Tarchini et al, 2013), *Gnai3* (Beer-Hammer et al, 2018; Ezan et al, 2013; Mauriac et al, 2017) or *Gnai2; Gnai3* (Beer-Hammer et al, 2018) were inactivated did not report symmetrical HC. In addition, mouse strains expressing ptxA *in vivo* also did not produce symmetrical cochlear HC (Tarchini et al, 2013; Tarchini et al, 2016).

Second, ptx experiments induced striking HC misorientation. In the cochlea, misorientation manifested as a 180° inversion of outer HC in the first and second row (OHC1-2) whereas inner HC (IHC) and OHC3 were much less affected (**Figure 1C**) (Ezan et al, 2013; Kindt et al, 2021; Tarchini et al, 2013). In the vestibular system, ptxA expression abrogated the line of polarity reversal and thus the mirror-image HC organization characteristic of macular organs, the utricle and saccule (Jiang et al, 2017; Kindt et al, 2021). Normal orientation reversal was also lost upon inactivating two endogenous mouse proteins: the transcription factor EMX2 in the maculae (Jiang et al, 2017) and the orphan GPCR GPR156 in cochlear OHC1-2 and in the maculae (Kindt et al, 2021). Together, these recent studies uncovered an EMX2>GPR156>GNAI signaling cascade that secures a normal pattern of HC orientation by reversing *Emx2*-positive HC. GNAI signals downstream of GPR156 to reverse the orientation of the basal body migration in *Emx2*-positive compared to *Emx2*-negative HC (Tona & Wu, 2020) (reviewed in (Tarchini, 2021)). While ptx impact on orientation thus appears to be physiologically relevant, HC misorientation was surprisingly not reported in single *Gnai3* or double *Gnai2; Gnai3* mutants (Beer-Hammer et al, 2018; Mauriac et al, 2017).

In summary, the importance of the GPSM2-GNAI complex for hair bundle development is well-established, but multiple discrepancies cast a doubt on whether GNAI proteins also assume earlier polarization roles. Specific questions include whether GNAI proteins participate in the mechanism that pushes the basal body away from the cell center, and in the distinct EMX2>GPR156 mechanism that makes a binary decision on the direction of this push (**Figure 1B**). Furthermore, it remains unclear whether GNAI2 and GNAI3 adopt similar or distinct distributions in HC, and whether GNAI1 or GNAO also participate in these processes.

In this study, we embarked on a systematic analysis of single and combined *Gnai1*, *Gnai2*, *Gnai3* and *Gnao1* mouse mutants to solve the actual role(s) of GNAI/O proteins during HC differentiation. Our results confirm that GNAI3 is the only GNAI/O protein required for normal hair bundle morphogenesis and normal auditory brainstem response (ABR) thresholds. In absence of GNAI3, GNAI2 can fully compensate at embryonic stages but is not enriched with GPSM2 long enough to ensure normal hair bundle morphogenesis at postnatal stages. We directly demonstrate that GNAI proteins have two early polarization roles independent of GPSM2 during embryogenesis. In sum, GNAI function is instrumental for HC to a) break planar symmetry, b) adopt a proper binary orientation along the PCP axis downstream of EMX2 and GPR156, and c) elongate and organize stereocilia into a functional hair bundle with GPSM2.

Results

A near-comprehensive collection of *Gnai/o* mouse mutants

In order to interrogate the individual and combined roles of all inhibitory G proteins during HC differentiation, we obtained or generated mouse strains to build a collection of single and double *Gnai/o* mutants. Single *Gnai1* and *Gnai3* mutants were derived from the *Gnai1*^{tm1Lbi}; *Gnai3*^{tm1Lbi} double mutant strain (hereafter *Gnai1*^{neo}; *Gnai3*^{neo}) (Jiang et al, 2002) by segregating individual mutations upon breeding (see Methods and **Supp. Table 1** for details on all strains). We generated a new constitutive *Gnai2* mutant strain (*Gnai2*^{del}) carrying a deletion of exons 2 to 4

(**Figure 2 Supp. 1A**; see Methods). Finally, we obtained and derived two *Gnao1* mutant strains: a constitutive inactivation allele where a neomycin cassette disrupts exon 6 (*Gnao1*^{neo}) (Jiang et al, 1998) and the conditional inactivation allele *Gnao1*$^{tm1c(EUCOMM)Hmgu}$ (hereafter *Gnao1*^{flox}). As simultaneous constitutive loss of GNAI1 and GNAI2 was reported as viable (Plummer et al, 2012), we established a *Gnai1*^{neo}; *Gnai2*^{del} double mutant strain in addition to *Gnai1*^{neo}; *Gnai3*^{neo} (Jiang et al, 2002). In contrast, double inactivation of *Gnai2; Gnai3* is lethal around Embryonic (E) day 10.5, before HC are born (Gohla et al, 2007). Consequently, we generated a new *Gnai3*^{flox} strain by flanking exons 2 and 3 with *loxP* sites (**Figure 2 Supp. 1B**; see Methods). We then generated conditional *FoxG1-Cre; Gnai2*^{del}*; Gnai3*^{flox} double mutants where *Gnai3* inactivation occurs as early as E8.5 in the otic vesicle (Hebert & McConnell, 2000). Investigating all *Gnai/o* strains in the same genetic background was unrealistic for feasibility and lethality reasons. We reasoned that apical HC development is probably highly constrained and less likely to be influenced by genetic heterogeneity compared to susceptibility to disease, for example.

As two of the three defects directly attributed to GNAI/O dysfunction were only observed using pertussis toxin (**Figure 1C**), the *Gnai/o* strains above needed to be compared to a strain expressing ptxA in HC. We used our *R26*$^{LSL\text{-}myc:ptxA}$ strain (hereafter *LSL-myc:ptxA*) expressing N-terminal myc-tagged ptxA upon Cre recombination (**Figure 2 Supp. 1C**) (Tarchini et al, 2016). Because a related *R26*$^{LSL\text{-}ptxAa:myc}$ strain carrying a C-terminal myc tag (Regard et al, 2007) caused milder HC misorientation defects than *LSL-myc:ptxA* in the vestibular system (Jiang et al, 2017; Kindt et al, 2021), we wondered whether the myc tag could weaken toxin activity even perhaps when located N-terminal. Consequently, we generated a new strain, *R26*$^{DIO\text{-}ptxA}$ (hereafter *DIO-ptxA*), where untagged ptxA is flanked by double-inverted *lox* sites and flipped from the non-coding to the coding strand upon Cre recombination (**Figure 2 Supp. 1D**; see Methods) (Schnutgen et al, 2003). In *DIO- ptxA*, *ptxA* expression is driven by a strong artificial CAG promoter, and not by the endogenous *R26* promoter as in previous strains (Regard et al, 2007; Tarchini et al, 2016). We bred *LSL-myc:ptxA* and *DIO-ptxA* either with *FoxG1*-Cre active in otic progenitors (Hebert & McConnell, 2000), or alternatively with *Atoh1-Cre* (Matei et al, 2005) to limit GNAI/O inhibition to post-mitotic HC. Supplementary Table 1 summarizes the strains used in this study, their origin, genetic background and viability.

Only GNAI3 is required for hair bundle morphogenesis yet GNAI2 participates

To investigate the role of individual GNAI/O proteins in HC development, we imaged hair bundles in 3-week-old mutant and control littermate mice at the mid-cochlear position using scanning electron microscopy (SEM). Single *Gnai1* or *Gnai2* mutants as well as double *Gnai1; Gnai2* mutants did not show overt defects in OHC or IHC (**Figure 2A**). In single *Gnai3* mutants by contrast, some OHC hair bundles appeared truncated, and IHC displayed variably shortened row 1 stereocilia as well as supernumerary stereocilia rows (**Figure 2A-B**), as previously described (Mauriac et al, 2017). The same defects were observed in double *Gnai1; Gnai3* mutants and, as reported previously, in the *LSL- myc:ptxA* model (**Figure 2A-B**) (Tadenev et al, 2019). A constitutive (*Gnao1*^{neo}) or conditional (*Atoh1-Cre; Gnao1*^{flox}) inactivation of *Gnao1* did not produce overt apical HC defects (**Figure 2 Supp. 1E-F**). Conditional inactivation of *Gnao1* also did not enhance defects in the *Gnai1; Gnai3* mutant background (**Figure 2 Supp. 1F**).

In addition, *myc:ptxA* expression inverted the orientation of OHC1-2s (**Figure 2A**), as expected since ptxA inactivates the EMX2>GPR156>GNAI signaling cascade that defines HC orientation along the PCP axis (Kindt et al, 2021; Tarchini et al, 2013; Tarchini et al, 2016). However, a defect in HC orientation was not observed in single *Gnai1*, *Gnai2*, *Gnai3* mutants, or in double *Gnai1*; *Gnai2* and *Gnai1*; *Gnai3* mutants (**Figure 2A**). Despite extensive breeding, we could only obtain one adult animal carrying a double *Gnai2; Gnai3* inactivation due to postnatal lethality (*FoxG1-Cre; Gnai2*$^{del/del}$*; Gnai3*$^{flox/flox}$; see **Supp. Table 1**). Remarkably, this unique specimen not only recapitulated stereocilia stunting and extra stereocilia rows observed in the *Gnai3*^{neo},

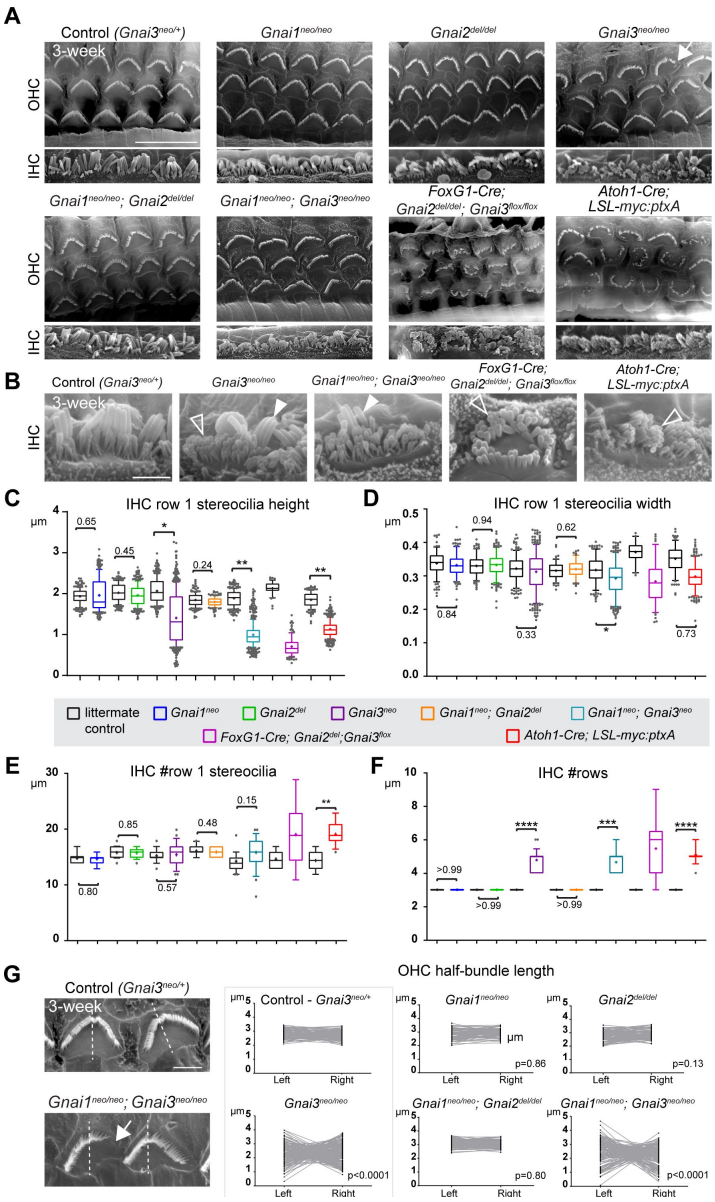

Figure 2.

Individual GNAI proteins make different contributions to hair bundle development.

A-B) SEM images of representative OHC (A) and IHC (B) in 3-week old animals at the cochlear mid. *Gnai1*^{neo}, *Gnai2*^{del}, and *Gnai1*^{neo}*; Gnai2*^{del} mutants show apparently normal hair bundles in both HC types. In contrast, *Gnai3*^{neo} and *Gnai1*^{neo}*; Gnai3*^{neo} mutants show defects in both HC types, including truncated hair bundles in OHC (arrow), as well as supernumerary rows of stunted (hollow arrowheads) or variable height stereocilia (full arrowheads) in IHC. In addition, in *FoxG1-Cre; Gnai2*^{del}*; Gnai3*^{flox} and *Atoh1-Cre; LSL-myc:ptxA* mutants, OHC1-2s are severely misoriented. **C-F)** Quantification of various hair bundle features in 3-week old IHC at the cochlear mid. Each mutant strain is compared to littermate controls (in black; exact genotypes detailed in Source Data file). At least 3 animals, 17 IHC and 108 stereocilia are represented per condition, except for *FoxG1-Cre; Gnai2*^{del}*; Gnai3*^{flox} where we could only obtain a single adult animal due to postnatal lethality. Nested (hierarchical) t-test sorted by animal; p<0.0001****, p<0.001***, p<0.01**, p<0.05*; non-significant p-values are indicated. Detailed cohort sizes and statistics can be found in Source Data file. **G)** SEM images of representative OHC showing a truncated hair bundle (arrow). Lengths of the left and right wing of the hair bundle were measured and plotted as paired values for the same OHC. A littermate control graph is only shown for *Gnai3* mutants (*Gnai3*$^{neo/+}$ controls). Littermate control graphs for the other mutants can be found in **Fig. 2 Supp. 1G**. p-values are for a F-test of variance of pooled left and right wing lengths compared to littermate controls. At least 3 animals and 88 OHC are represented per genotype. Only *Gnai3* and *Gnai1*; Gnai3 mutants show truncated hair bundles and a significant p value (p<0.05). Scale bars are 10µm (A) and 2µm (B, G). OHC, outer hair cell; IHC, inner hair cell.

Gnai1^{neo}*; Gnai3*^{neo} and *LSL-myc:ptxA* models (**Figure 2A-B**), but apparently also OHC1-2 misorientation only observed to date in the *LSL-myc:ptxA* and *Gpr156* mutants (**Figure 2A**) (Kindt et al, 2021). This result suggests that endogenous GNAI proteins are involved in HC orientation, and that GNAI2 can function in the EMX2>GPR156>GNAI signaling cascade to secure proper OHC1-2 orientation in *Gnai1; Gnai3* double mutants. This point is verified and expanded below when neonate HC orientation is addressed.

To acquire a quantitative view of *Gnai* mutant defects and help comparisons, we first focused on IHC and measured row 1 stereocilia height and width, as well as the number of stereocilia in row 1 and the number of rows in the bundle in all strains (**Figure 2C-F**). This analysis uncovered a *Gnai3*^{neo} < *Gnai1*^{neo}*; Gnai3*^{neo} < *LSL-myc:ptxA* < *FoxG1-Cre; Gnai2*^{del}*; Gnai3*^{flox} allelic series along which a) defects increased in severity, as manifested by increased variability and decreased averages (row 1 height; **Figure 2C**), and b) new defects appeared (excess row 1 stereocilia only observed in *LSL-myc:ptxA and Gnai2*^{del}*; Gnai3*^{flox}; **Figure 2E**). The phenotypic series moved towards increasingly immature-looking hair bundles, and increasingly mimicked severe defects in *Gpsm2* mutants (Mauriac et al, 2017; Tadenev et al, 2019; Tarchini et al, 2016).

To quantify and compare hair bundle truncations in OHC, we measured the length of the half-bundle 'wings' on each side of the central vertex. We limited this analysis to mutant strains where hair bundles retained a recognizable vertex, thus excluding *LSL-myc:ptxA* and *FoxG1-Cre; Gnai2*^{del}*; Gnai3*^{flox}. We then plotted paired left and right values for each OHC and tested length variance for each mutant (**Figure 2G**; **Figure 2 Supp. 1G**). In *Gnai1*, *Gnai2* and *Gnai1; Gnai2* mutants, the two wings of each hair bundle had similar lengths, and variance was similar to control littermates. In contrast, variable truncation of one wing in *Gnai3* and *Gnai1; Gnai3* mutants resulted in significantly higher length variance compared to controls (**Figure 2G**; **Figure 2 Supp. 1G**). In both *Gnai3* and *Gnai1; Gnai3* mutants, 49% of hair bundles had wings of more different lengths than the worst OHC outlier in littermate controls (see Source Data file).

In conclusion, all GNAI/O proteins are not equally involved in hair bundle morphogenesis, with GNAI3 playing a particularly prominent role. GNAI2 makes a clear contribution since *Gnai3* mutant stereocilia defects dramatically increase in severity when GNAI2 is also absent in *Gnai2; Gnai3* double mutants. These results confirm previous conclusions (Beer-Hammer et al, 2018). In addition, we largely rule out that GNAO is involved in apical HC differentiation. More severe defects in *Gnai1; Gnai3* double mutants compared to *Gnai3* single mutants may indicate that GNAI1 plays a subtle role. However, we cannot rule out differences in genetic background as the underlying cause since *Gnai3*^{neo} is in mixed (29S1/SvImJ; C57BL/6J) and *Gnai1*^{neo}*; Gnai3*^{neo} is in pure 129S1/SvImJ background (**Supp. Table 1**). GNAI1 thus has at best a minimal role in hair bundle development.

Only GNAI3 is required for normal auditory brainstem thresholds

To pair morphological defects with auditory function, we next tested Auditory Brainstem Response (ABR) in mutants and control littermates at 3 to 4 weeks of age. Anesthetized animals were presented with pure tone stimuli of decreasing sound pressure intensity (dB SPL) at 8, 16, 32 and 40 kHz and ABRs were recorded with a subcutaneous probe (see Methods). Mirroring their overtly normal apical HC morphology, *Gnai1*, *Gnai2* and *Gnai1; Gnai2* mutants showed thresholds comparable to littermate controls at all frequencies (**Figure 3A-C**). Similarly, constitutive (*Gnao1*^{neo}) or conditional (*Atoh1-Cre; Gnao1*^{flox}) loss of GNAO did not alter ABR thresholds (**Figure 3 Supp. 1A-B**). In contrast, *Gnai3* mutants were profoundly deaf at 32 and 40 kHz and displayed significantly elevated thresholds at 8 and 16 kHz compared to littermate controls (**Figure 3D**). *Gnai1; Gnai3* double mutants shared a similar ABR profile as *Gnai3* single mutants, with apparently higher thresholds at 8 and 16 kHz although these two strains were not compared as littermates (**Figure 3D**). Littermate controls for *Gnai1; Gnai3* double mutants were homozygote for *Gnai1*^{neo}(*Gnai1*$^{neo/neo}$*; Gnai3*$^{neo/+}$) and appeared to have higher thresholds than littermate controls for *Gnai3* mutants (*Gnai3*$^{neo/+}$) at 32 and 40 but not 8 and 16 kHz, whereas loss of GNAI1

did not impact auditory thresholds on its own (**Figure 3A**). These results match possibly more severe hair bundle defects when GNAI1 is inactivated along with GNAI3 (**Figure 2C-F**), and here again, could reflect either a difference in genetic background or a limited role for GNAI1.

In summary, we confirm that GNAI3, but not GNAI2, is essential for proper auditory thresholds, as previously proposed (Beer-Hammer et al, 2018). We also clarify that GNAO does not participate. Beer-Hammer and colleagues previously showed that inactivating GNAI2 worsens hearing loss in the *Gnai3* null background, as tested in their *FoxG1-Cre; Gnai2*$^{flox/flox}$*; Gnai3*$^{flox/flox}$ adults (Beer-Hammer et al, 2018). Using a comparable yet distinct model (*FoxG1-Cre; Gnai2*$^{del/del}$*; Gnai3*$^{flox/flox}$), we were largely unable to obtain young adults and thus could not perform ABR. This suggests that our model is more severely affected, and would probably lack ABRs, similar to *FoxG1-Cre; Gnai2*$^{flox/flox}$*; Gnai3*$^{flox/flox}$ (Beer-Hammer et al, 2018) and *LSL-myc:ptxA* (Tarchini et al, 2016).

Distribution of individual GNAI proteins in neonate hair cells

Next, we attempted to define how individual GNAI/O proteins localize in neonate HC. GNAI/O proteins are close paralogs, with mouse and human GNAI1 and GNAI3 most similar in the GNAI group, and GNAO more divergent compared to all GNAI (**Figure 1A**). Validating and using specific antibodies would thus be challenging. Instead, we used one commercial antibody raised against GNAI3 (scbt"GNAI3") and one antibody raised against GNAI2 (pt"GNAI2") and systematically immunolabeled our mouse model collection to tease apart protein-specific behavior.

Both antibodies produced the familiar GNAI pattern of enrichment at the bare zone and at row 1 stereocilia tips (**Figure 4**; arrows and arrowheads, respectively) (Tarchini et al, 2013; Tarchini et al, 2016). Both antibodies revealed generally normal GNAI enrichment in *Gnai1* (**Figure 4A**), *Gnai2* (**Figure 4B**), and *Gnai1*; *Gnai2* mutants (**Figure 4C**). This indicates that pt"GNAI2" is not specific for GNAI2 and can also detect GNAI3. In *Gnai3* and *Gnai1; Gnai3* mutants, both antibodies still detected GNAI protein at the bare zone and at stereocilia tips although some HC displayed incomplete enrichment (**Figure 4D**- E; detailed analysis below, **Figure 5**). This indicates that scbt"GNAI3" is not specific for GNAI3 and can also detect GNAI2. Finally, neither antibody detected consistent signal over background in *Gnai2; Gnai3* double mutants where GNAI1 is the only GNAI protein remaining (**Figure 4F**; *FoxG1-Cre; Gnai2*$^{del/del}$*; Gnai3*$^{flox/flox}$). To test experimentally whether these antibodies can detect GNAI1, we first electroporated *Gnai1*, *Gnai2* or *Gnai3* constructs in E13.5 inner ears and cultured the cochlea for 6 days before immunolabeling. Overexpressed *Gnai1* was efficiently detected by pt"GNAI2" but not by scbt"GNAI3" whereas, as expected, overexpressed *Gnai3* was detected by scbt"GNAI3" (**Figure 4 Supp. 1A**). We next used pt"GNAI2" to immunolabel the gallbladder epithelium where *Gnai1* expression was specifically reported (*mousephenotype.org*; *LacZ* reporter in *Gnai1*$^{tm1a(EUCOMM)Wtsi}$ strain). Signals were visibly reduced in *Gnai1* mutants compared to littermate controls (**Figure 4 Supp. 1B**).

Together, these results indicate that a) GNAI2 and GNAI3 share the same polarized distribution pattern at the bare zone and at stereocilia tips, and b) GNAI1 is absent or hidden by background signals at the HC apical surface since it can be detected by the pt"GNAI2" antibody in other contexts. Loss of GNAO in the *Gnao1*^{neo}or *Atoh1-Cre; Gnao1*^{flox} models did not alter signals obtained with scbt"GNAI3" (**Figure 4 Supp. 1C-D**). Moreover, a GNAO antibody produced unpolarized apical signals that proved unspecific since they were unchanged in *Atoh1-Cre; Gnao1*$^{flox/flox}$ mutants (**Figure 4 Supp. 1E**). Thus, GNAO likely does not contribute to HC polarization, as also suggested by normal hair bundles and normal ABR thresholds in *Gnao1* mutants.

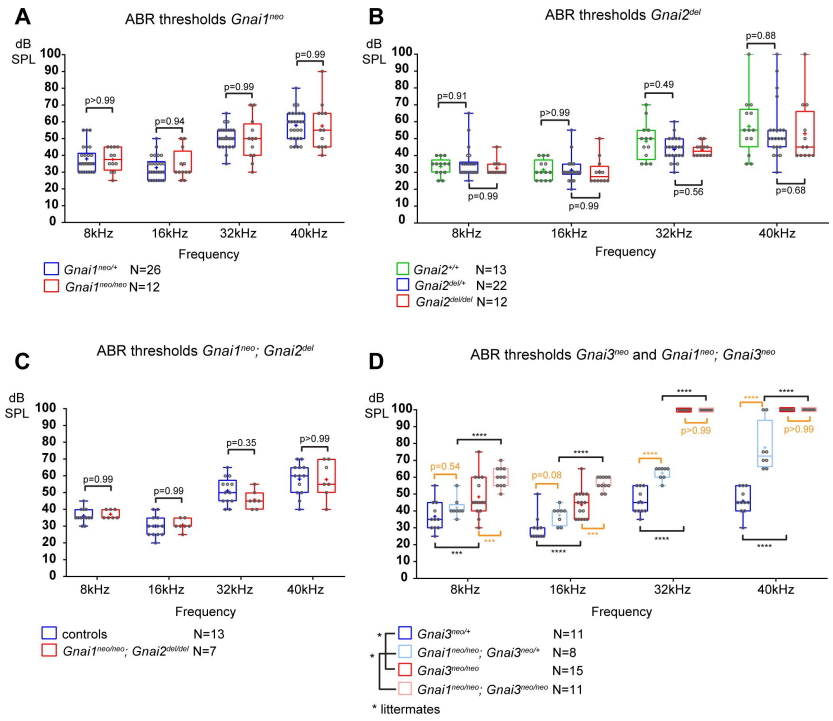

Figure 3.

Loss of GNAI3 leads to hearing loss most severe at high frequencies.

A-D) ABR thresholds at 8, 16, 32, and 40 kHz for *Gnai1*^{neo} (A), *Gnai2*^{del} (B), *Gnai1*^{neo}*; Gnai2*^{del} (C), and *Gnai3*^{neo} and *Gnai1*^{neo}*; Gnai3*^{neo} (D) mutants tested between P21 and P29. Boxplots are framed with 25-75% whisker boxes where exterior lines show the minimum and maximum values, the middle line represents the median, and + represent the mean. A plotted value of 100 dB indicates animals that did not respond to 90 dB stimuli. In (C), controls are a pool of *Gnai1*$^{+/+}$*; Gnai2*$^{del/+}$, *Gnai1*$^{neo/+}$*; Gnai2*$^{+/+}$ and *Gnai1*$^{neo/+}$*; Gnai2*$^{del/+}$ animals. N indicates the number of animals of both sexes tested. Two-way ANOVA with Sidak's multiple comparison. p<0.0001****, p<0.001***; non-significant p-values are indicated. p-values in orange were obtained comparing non-littermate animals and suggest possibly raised thresholds when GNAI1 is inactivated in addition to GNAI3, or due to a difference in genetic background (see text). kHz, kiloHertz, dB SPL, decibel sound pressure level.

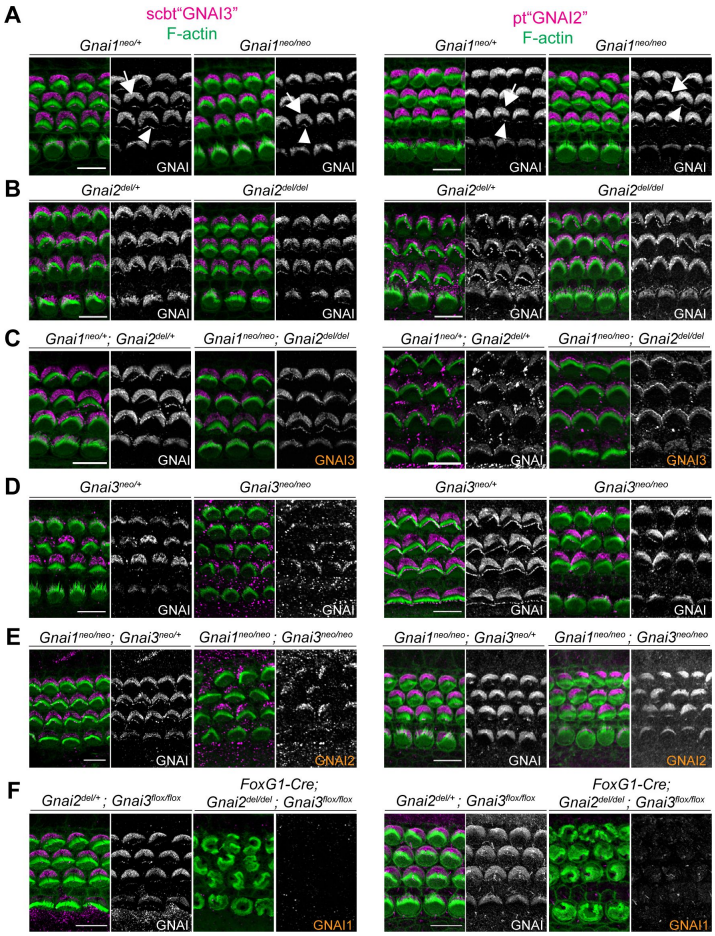

Figure 4.

Systematic immunolabeling of GNAI proteins in *Gnai* mutant strains.

A-F) Two different antibodies (scbt"GNAI3" and pt"GNAI2") were used to label the auditory epithelium at P0-P3. GNAI proteins were detected at the bare zone (arrows) and at stereocilia tips (arrowheads). Neither antibody is specific for its protein target, as scbt"GNAI3" is able to detect GNAI2 (E) and pt"GNAI2" is able to detect GNAI3 (C). Note how no apical GNAI signal is visible with either antibody in *Gnai2; Gnai3* double mutants (F), showing that GNAI1 is not enriched apically in HC (see **Fig. 4 Supp. 1A-B** for evidence that pt"GNAI2" detects GNAI1). When the identity of the GNAI protein detected is unambiguous based on genotype, it is made explicit in orange. Scale bars are 10µm.

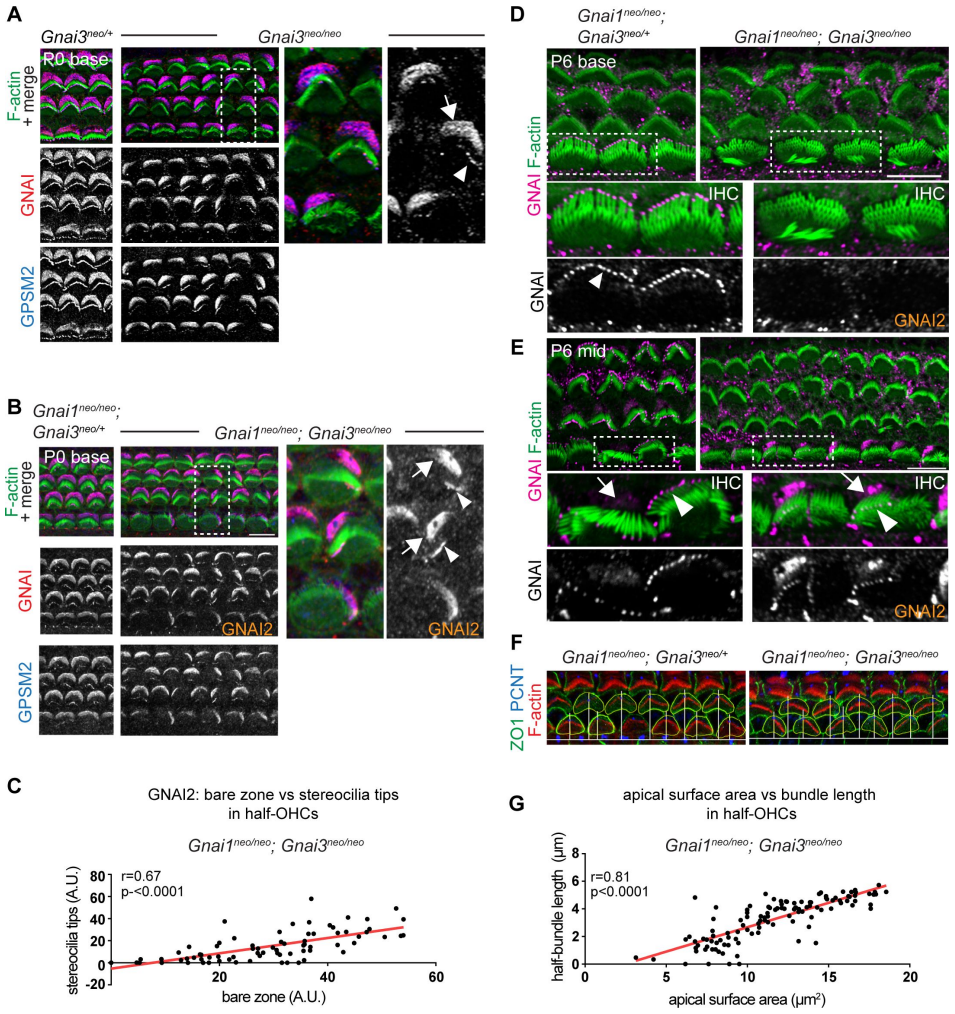

Figure 5.

GNAI2 only partially rescues loss of GNAI3 in individual postnatal hair cells.

A-B) GNAI (pt"GNAI2" antibody; see **Fig. 4**) and GPSM2 co-immunolabeling in P0 *Gnai3*^{neo} (A) and *Gnai1*^{neo}*; Gnai3*^{neo} (B) animals at the cochlear base. Boxed regions are magnified on the right. In both mutants, incomplete GNAI patterns are observed at the bare zone (arrow) and stereocilia tips (arrowheads). Remaining GNAI signals must reflect GNAI2 in (B). **C)** Correlation plot of GNAI signal intensity at the bare zone and tips in half-OHC at the P2 cochlear mid. Presence or absence of GNAI is remarkably correlated spatially between bare zone and tips in the same half-OHC. N=3 animals, n=37 OHC, Pearson correlation with best fit (red line; plot for control littermates can be found in **Fig. 5 Supp. 1A**). **D-E)** GNAI (pt"GNAI2" antibody) immunolabeling in P6 *Gnai1*^{neo}*; Gnai3*^{neo} animals. Boxed IHC regions are magnified below. Loss of GNAI2 progresses with HC differentiation, with largely absent IHC signals at the P6 cochlear base (D) but partial rescue on one side of the cell at the P6 mid (E), as observed at the cochlear base at P0 (A-B). **F)** ZO1 (apical junctions) and pericentrin (PCNT; basal body) immunolabeling in P8 OHC (maximum projection). The position of the basal body is used to determine the vertex (middle) of the original hair bundle and to draw a radial line separating each OHC into two halves. **G)** The length of each hair bundle wing (y axis) is graphed in relation to the corresponding apical surface area (x axis) in the same half-OHC. Truncated OHC wings correlate with reduced apical membrane area on the same side. N=3 animals, n=58 OHC, Pearson correlation with best fit (red line; plot for control littermates can be found in **Fig. 5 Supp. 1C**). A.U., arbitrary unit. Scale bars are 10µm.

GNAI2 only partially spans the bare zone and stereocilia tips and partially rescues hair bundle development in postnatal hair cells lacking GNAI3

We next took a closer look at incomplete GNAI enrichment in *Gnai3* and *Gnai1; Gnai3* mutant HC (**Figure 4D-E**). In both models, we observed an identical outcome at the P0 cochlear base where remaining GNAI was unable to fully and consistently occupy the HC sub-domains when GNAI3 was missing (**Figure 5A-B**; bare zone, arrows; stereocilia tips, arrowheads). In *Gnai1;* Gnai3 double mutants, the GNAI protein detected is by default GNAI2, and this is likely also true in single *Gnai3* mutants since GNAI1 is not observed in HC (**Figure 4F**). Because in all cases GPSM2 co-localized with GNAI2 (**Figure 5A-B**), these results demonstrate that both GNAI2 and GNAI3 can form a complex with GPSM2 in HC. Intriguingly, the absence of GPSM2-GNAI2 on one side of the bare zone at P0 appeared to coincide with its absence at stereocilia tips on the corresponding side (**Figure 5A-B**). We thus quantified GNAI2 intensity at the bare zone and at stereocilia tips in half-OHC in *Gnai1; Gnai3* mutants. While as expected control OHC showed little variation in GNAI enrichment in either compartment (**Figure 5 Supp. 1A**), mutant OHC showed highly variable signals that were significantly correlated between the bare zone and tips in the same half-OHC (**Figure 5C**). Analyzing HC at different stages and tonotopic positions clarified that GNAI2 is progressively unable to compensate for missing GNAI3. At E18.5, the GPSM2-GNAI2 complex could still occupy the totality of the bare zone in *Gnai1; Gnai3* mutants (**Figure 5 Supp. 1B**), suggesting that GNAI2 fully compensates for the loss of GNAI3 in embryonic HC. At later stages of HC differentiation, partial compensation by GNAI2 observed at P0 (**Figure 5A-C**) evolved into a lack of compensation by P6 at the cochlear base, where GNAI2 was no longer detected consistently at the tips of stunted stereocilia in mutant IHC (**Figure 5D**). In contrast, less mature P6 IHC at the cochlear mid position retained partial GNAI2 enrichment correlated between the bare zone and tips (**Figure 5E**), as seen at P0 (**Figure 5A-B**).

The progressive inability of GNAI2 to cover for GNAI3 in individual HC helps explain the unique profile of apical defects in *Gnai3* and *Gnai1; Gnai3* mutants. Loss of GPSM2- GNAI2 in one wing of the OHC hair bundle led to stereocilia degeneration by P8 (**Figure 5F**). One-sided loss of global GNAI function at stereocilia tips is thus likely the origin of truncated hair bundle wings observed in adults *Gnai3* and *Gnai1; Gnai3* mutant OHC (**Figure 2G**). We divided the P8 OHC apical surface in two halves based on the position of the basal body at the hair bundle vertex, and measured the length of each hair bundle wing as well as the total apical surface area in the same HC half in *Gnai1; Gnai3* mutants (**Figure 5F**). We found a significant correlation between these two values (**Figure 5G**; control graph in **Figure 5 Supp. 1C**), providing further evidence that loss of stereocilia prompts a corresponding loss of flat HC surface area on the same OHC side (Etournay et al, 2010). Finally, we asked whether in time GNAI2 is lost in all stereocilia and along the entire cochlea in *Gnai1; Gnai3* mutants. This proved not to be the case, as GNAI2 could still be detected at stereocilia tips in P28 OHC and IHC, although in low and variable amounts compared to GNAI tip signals in littermate controls (**Figure 5 Supp. 1D-E**).

In conclusion, GNAI2 could provide a low dose of GNAI protein at stereocilia tips when GNAI3 is missing and preserve elongation and height to some extent. Variable GNAI2 amounts thus likely explain why IHC stereocilia have variably reduced heights in absence of GNAI3 (**Figure 2B-C**; **Figure 5D-E**), unlike in *Gpsm2* or *LSL-myc:ptxA* mutants where they are more uniformly stunted (Beer-Hammer et al, 2018; Mauriac et al, 2017; Tadenev et al, 2019; Tarchini et al, 2016). Loss of GNAI2 signals that coincides at the bare zone and at stereocilia tips on the same HC side adds to previous evidence suggesting that bare zone enrichment is essential for GPSM2-GNAI trafficking to adjacent row 1 stereocilia (Akturk et al, 2022; Jarysta & Tarchini, 2021; Tarchini et al, 2016).

Combined loss of GNAI2 and GNAI3 delays and de-polarizes bare zone expansion with drastic consequences on stereocilia distribution

Since GNAI2 and GNAI3 show functional redundancy and are the most important GNAI/O proteins for hair bundle differentiation, we next focused on characterizing early HC development in *Gnai2; Gnai3* double mutants (*Foxg1-Cre; Gnai2*$^{del/del}$*; Gnai3*$^{flox/flox}$) and comparing defects to those observed previously with ptx. Unlike at adult stages, *Gnai2; Gnai3* double mutants were obtained in close to Mendelian proportions at P0 (see **Supp. Table 1**). For this goal, we used the new *DIO-ptxA* allele in case the myc tag hindered ptxA activity in the *LSL-myc:ptxA* allele. We first validated the new *Gnai3*^{flox} *and DIO-ptxA* alleles (**Figure 2 Supp. 1B, D**). As expected, GNAI signals at the bare zone and stereocilia tips were normal in *Gnai3*$^{flox/flox}$ homozygotes but showed a distinctive incomplete pattern along with stunted stereocilia upon Cre recombination (**Figure 6 Supp. 1A**), as in constitutive mutants (**Figure 5A**). In fact, the new *DIO-ptxA* model produced identical apical HC defects to the earlier *LSL-myc:ptxA* strain in single HC (Kindt et al, 2021; Tarchini et al, 2016) (**Figure 6 Supp. 1B**). The fraction of inverted OHC1 in the *DIO-ptxA* model was lower than in the *LSL-myc:ptxA* model when using the postmitotic HC driver *Atoh1-Cre* (**Figure 6 Supp. 1C**) but identically encompassed 100% of OHC1 with the early *FoxG1-Cre* driver (**Figure 6 Supp. 1D**). Similar apical HC defects between strains indicate that the N-terminal myc tag and mild *R26* promoter do not limit ptxA activity in *LSL- myc:ptxA*. For comparison purposes, we used the *FoxG1-Cre* driver to inactivate GNAI2/GNAI3 and to express ptxA, the same driver used by Beer-Hammer and colleagues (Beer-Hammer et al, 2018).

Inactivating GNAI2 and GNAI3 abolished the bare zone at E17.5 based on abnormally uniform F-actin signals at the HC surface compared to controls where low F-actin matched GNAI signals (**Figure 6A-B**; arrows point to the bare zone). In contrast, E17.5 *DIO-ptxA* HC had developed a distinct bare zone (**Figure 6C**, arrows). Measuring its surface area by HC type confirmed that the bare zone was virtually absent in *Gnai2; Gnai3* double mutants but only trended as reduced in ptxA-expressing OHC (**Figure 6D**). By P0, most *Gnai2; Gnai3* mutant HC at the cochlear base had developed a region lacking microvilli or stereocilia, but its position at the apical surface was highly irregular, complementing extremely dysmorphic hair bundles (**Figure 6E-F**; arrows point to bare regions). In contrast, P0 *DIO-ptxA* HC displayed largely coherent hair bundles and a polarized bare zone (**Figure 6G**, arrows). Quantifications revealed a significantly reduced bare area in P0 *Gnai2; Gnai3* mutants compared to littermate controls (**Figure 6H**), showing that bare zone emergence and expansion is greatly delayed and deregulated in this model (compare P0 in **Figure 6H** and E17.5 in **Figure 6D**). In P0 *DIO-ptxA* HC, the bare zone surface area was largely comparable to controls, suggesting that a slight delay in expansion is progressively corrected in time in this model (compare P0 in **Figure 6H** and E17.5 in **Figure 6D**). These results best illustrate to date the importance of GPSM2- GNAI for bare zone emergence, expansion and polarized positioning. While both mutant models consistently delay bare zone expansion, differences in timing and severity suggest that ptxA is not as effective as the *Gnai2; Gnai3* double mutant to inhibit GPSM2- GNAI function. This is further underscored by severe stereocilia distribution defects observed in *Gnai2; Gnai3* but not *DIO-ptxA* mutants.

As reported previously (Kindt et al, 2021; Tarchini et al, 2013; Tarchini et al, 2016), the orientation of OHC1-2 expressing ptxA was inverted compared to controls (**Figure 6C**, G). Our single *Gnai2; Gnai3* adult mutant sample also appeared to have inverted OHC1 based on hair bundle morphology (**Figure 2A**). However, HC orientation proved challenging to assess in neonate *Gnai2; Gnai3* mutants due to highly dysmorphic hair bundles (**Figure 6A-B**; E-F). We thus used acetylated tubulin (AcTub) and pericentrin (PCNT) as markers for the kinocilium and the basal body, respectively. This showed that in *Gnai2; Gnai3,* but not in *DIO-ptxA* mutants, the basal

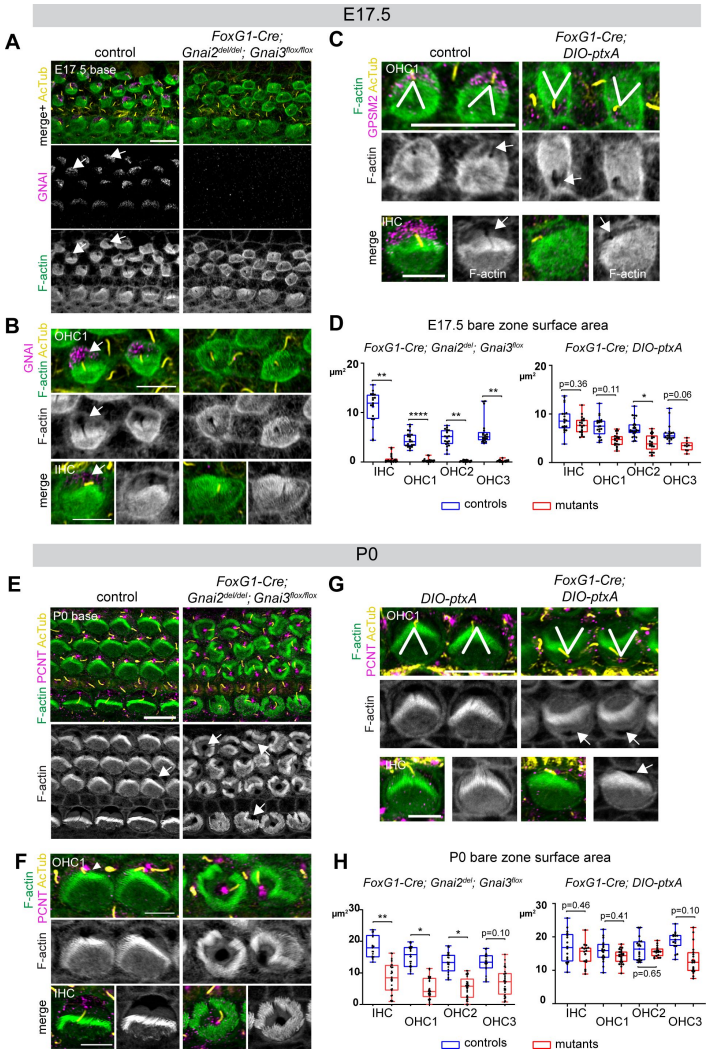

Figure 6.

Delayed bare zone expansion and severely dysmorphic hair bundles in absence of GNAI2 and GNAI3.

A-B) GNAI (scbt"GNAI3" antibody, see **Fig. 4**) and acetylated tubulin (AcTub; kinocilium) co-immunolabeling at the E17.5 cochlear base. Note how F-actin labeling (phalloidin) reveals a polarized bare zone marked by GNAI (arrows) in control but not in *Gnai2; Gnai3* double mutants. **C)** GPSM2 and AcTub co-immunolabeling at the E17.5 cochlear base. In contrast to *Gnai2; Gnai3* double mutants (A-B), *FoxG1-Cre; DIO-ptxA* mutants have a polarized bare zone (arrows) despite OHC1- 2 adopting a reversed orientation (V brackets indicate OHC1 orientation). GPSM2 marks the bare zone in controls and is reduced in mutants. **D)** Graphs of bare zone surface area in E17.5 HC at the cochlear base. *FoxG1-Cre; Gnai2^{del}; Gnai3^{flox}*: controls (*Gnai2$^{del/+}$; Gnai3$^{flox/+}$* and *Gnai2$^{del/+}$; Gnai3$^{flox/ flox}$*) N=3 animals, n=19 IHC, 23 OHC1, 19 OHC2, 21 OHC3; mutants N=3, n=23 IHC, 24 OHC1, 23 OHC2, 24 OHC3. *FoxG1-Cre; DIO-ptxA*: controls (Cre-negative *DIO-ptxA*) N=3, n=18 IHC, 18 OHC1, 21 OHC2, 18 OHC3; mutants N=3, n= 21 IHC, 20 OHC1, 21 OHC2, 9 OHC3. **E-G)** Pericentrin (PCNT) and AcTub co-immunolabeling at P0 at the cochlear base. Unlike at E17.5 (A-B, D), most P0 *Gnai2; Gnai3* double mutant HC have a bare region (E-F, arrows). This bare region is unpolarized and its abnormal shape reflects aberrant stereocilia distribution. In sharp contrast, ptxA mutants have normally shaped hair bundles and bare zones despite OHC1-2 adopting a reversed orientation (G). **H)** Graphs of bare zone surface area in P0 HC at the cochlear base. *FoxG1-Cre; Gnai2^{del}; Gnai3^{flox}*: controls (*Gnai2$^{del/+}$; Gnai3$^{flox/+}$*, *Gnai2$^{del/+}$; Gnai3$^{flox/flox}$* and *FoxG1-Cre; Gnai2$^{del/+}$; Gnai3$^{flox/+}$*) N=3, n=19 IHC, 23 OHC1, 21 OHC2, 21 OHC3; mutant N=3, n=21 IHC, 22 OHC1, 24 OHC2, 24 OHC3. *FoxG1-Cre; DIO-ptxA:* controls (Cre-negative *DIO-ptxA*) N=3, n=15 IHC, 23 OHC1, 18 OHC2, 15 OHC3; mutants N=3, n= 16 IHC, 24 OHC1, 18 OHC2, 19 OHC3. D, H: Nested (hierarchical) t-test sorted by animal; p<0.01**, p<0.05 *; non-significant p-values are indicated. All *ptxA* samples are heterozygotes (*R26$^{DIO-ptxA/+}$*). Scale bars are 10µm (A, C (OHC), E, G (OHC)) and 5µm (B, C (IHC), F, G (IHC)).

body and kinocilium were often in an approximately central position surrounded partially or entirely by stereocilia (**Figure 6E-F**). Rounded perinatal hair bundles are a hallmark of HC where the early off-center migration of the basal body, hence symmetry breaking, is defective.

To distinguish symmetry-breaking from HC orientation, we next used the position of the basal body at the base of the kinocilium to derive both HC eccentricity and HC orientation. This strategy helped compare the *Gnai2; Gnai3* and *DIO-ptxA* mouse models, and identified two early functions for GNAI before its association with GPSM2 for stereocilia elongation.

GNAI proteins drive the off-center migration of the basal body

We used the position of the basal body to measure HC eccentricity as a metric for cytoskeleton asymmetry. Eccentricity was calculated as a ratio reporting how far away from the cell center the basal body was positioned (see schematic in **Figure 7**). A perfectly symmetrical HC with a central basal body would thus have an eccentricity close to 0 whereas a ratio close to 1 would indicate that the off-center basal body is juxtaposed to the apical junction. Because HC maturation progresses in time and along the tonotopic axis (cochlear apex to base gradient of increasing maturity), we measured eccentricity at E17.5 (base and mid cochlear position) and at P0 (base, mid and apex) to understand how eccentricity progressed at the HC population level.

Control HC at E17.5 had already broken symmetry at the mid position, with eccentricity averaging ~0.5 and increasing at the more mature base position (**Figure 7A**). At E17.5 mid and base positions, *Gnai2; Gnai3* mutant HC showed a significantly reduced eccentricity, suggestive of a delay in the off-center migration of the basal body. We arbitrarily defined 0.25 as a threshold below which HC were considered near-symmetrical. Symmetrical HC were not observed in controls but represented up to ~29% of IHC and ~34% of OHC in *Gnai2; Gnai3* mutants at E17.5 (detailed in **Figure 7A** by stage, position and HC type; red highlights). By P0, the proportion of symmetrical cells in mutants had decreased at all positions for OHC (3.3-15.2%), but remained high or increased for IHC (21.5-42.4%; **Figure 7A**).

The situation was radically different in the *DIO-ptxA* model. First, no symmetrical HC was observed at any stage or position in mutants (**Figure 7B**). In the *DIO-ptxA* model, the distribution of eccentricity values in IHC was generally similar to controls. By contrast, OHC eccentricity trended as higher in *DIO-ptxA* compared to littermate controls, with the difference becoming less significant with OHC differentiation (**Figure 7B**). Defective bare zone expansion (**Figure 6D**, H) can help explain the distinct eccentricity defects in the *DIO-ptxA* (transiently higher eccentricity) and *Gnai2; Gnai3* (lower eccentricity) mouse models. The position of the basal body is the sum of two opposite movements (**Figure 1B**): a) the early off-center migration that brings the basal body in the vicinity of the lateral junction, and b) the subsequent relocalization towards the cell center upon bare zone expansion that brings the basal body in contact with the forming hair bundle (Tarchini et al, 2013). In *DIO-ptxA*, transiently increased eccentricity in OHC is likely the outcome of a normal off-center basal body migration combined with delayed bare zone expansion (**Figure 6D**, H). In *Gnai2; Gnai3* mutants by contrast, decreased eccentricity in OHC (**Figure 7A**) stems from defective off-center migration of the basal body combined with an initially absent (E17.5), and then reduced (P0), bare region (**Figure 6D**, H). When an unpolarized bare region eventually emerges in *Gnai2; Gnai3* mutants (**Figure 6H**), it impacts basal body position without directionality, leading to highly variable eccentricity values compared to controls (**Figure 7A**), and thus variably dysmorphic hair bundles. The apparent increase in symmetrical IHC over time in *Gnai2; Gnai3* mutants (**Figure 7A**) may result from the delayed expansion of the bare region, which will relocalize the basal body centrally in a proportion of IHC.

In conclusion, symmetry-breaking (**Figure 7**), bare zone emergence and expansion and stereocilia distribution (**Figure 6**) are all severely impaired in *Gnai2; Gnai3* mutants. In ptxA mutants in contrast, symmetry-breaking occurs normally, bare zone expansion is only delayed and stereocilia distribution is less affected. It follows that ptxA does not achieve a loss of GNAI2/GNAI3

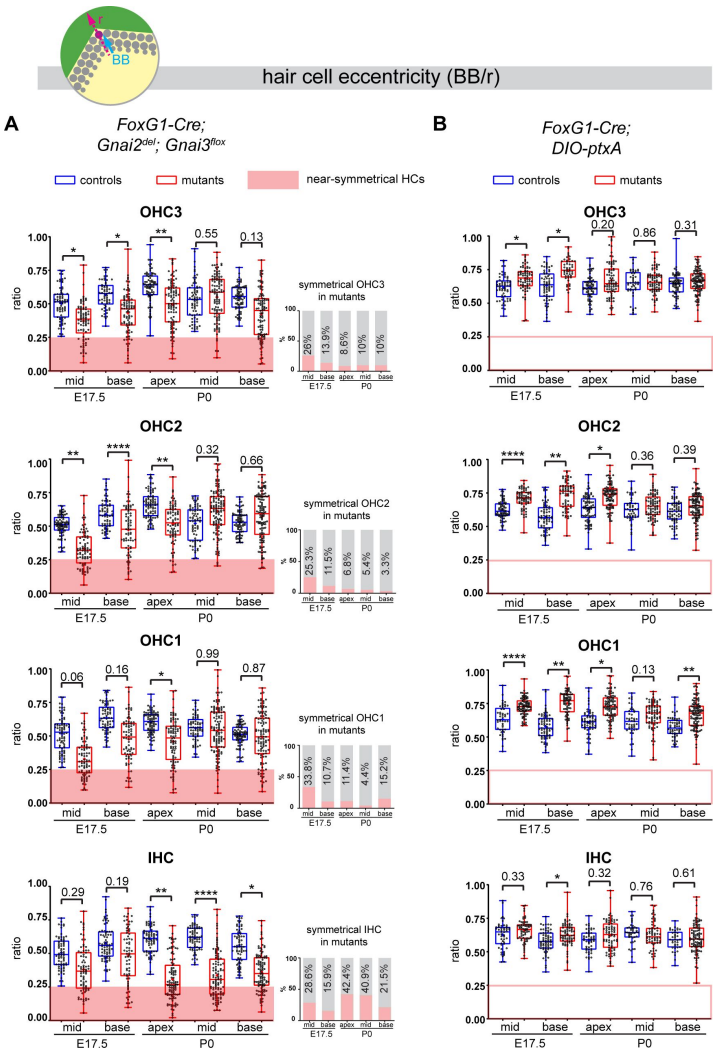

Figure 7.

Loss of GNAI2 and GNAI3 provokes hair cell eccentricity defects absent in *ptxA* mutants.

A-B) Graphs of HC eccentricity representing the position of the basal body as a ratio of the radius (BB/r, top diagram). Data cover E17.5 mid and base and P0 apex, mid and base cochlear positions for each HC type. HC were considered near-symmetrical when their eccentricity ratio was lower than 0.25 (red zone). Only *FoxG1-Cre; Gnai2*^{del}*; Gnai3*^{flox} mutants harbor symmetrical HC. Their proportion is indicated in the bar graphs on the right (A). Overall, the proportion of symmetrical cells tends to decrease in maturing OHC but remains high or increases in IHC. At least 3 animals and 39 cells per HC type are represented for each stage, cochlear position and genotype (detailed in Source Data file). Controls for *FoxG1-Cre; Gnai2*$^{del/del}$*; Gnai3*$^{flox/flox}$ are *Gnai2*$^{del/+}$*; Gnai3*$^{flox/+}$, *Gnai2*$^{del/+}$*; Gnai3*$^{flox/flox}$, *FoxG1-Cre; Gnai2*$^{del/+}$*; Gnai3*$^{flox/+}$ and *FoxG1-Cre; Gnai2*$^{del/+}$*; Gnai3*$^{flox/flox}$. Controls for *FoxG1-Cre; DIO- ptxA* are Cre-negative *DIO-ptxA* heterozygotes. Nested (hierarchical) t-test sorted by animal; p<0.0001 ****, p<0.01 **, p<0.05 *; non-significant p-values are indicated. Detailed cohort sizes and statistics can be found in Source Data file.

function as extensive as in *FoxG1-Cre; Gnai2; Gnai3* mutants. This is probably because ptxA only downregulates and does not inactivate GNAI/O proteins, and because ptxA substrates also include GNAI1 and GNAO that could be active in other contexts than polarization in HCs.

GNAI proteins orient hair cells laterally

GNAI proteins were proposed to signal downstream of the GPR156 receptor to regulate HC orientation in auditory and vestibular organs (Jiang et al, 2017; Kindt et al, 2021). In HC expressing the transcription factor EMX2, GPR156-GNAI reverses the orientation of the off-center basal body migration, and thus HC orientation, compared to *Emx2*-negative HC (Tona & Wu, 2020). To date, however, the HC misorientation profile observed in *Emx2* or *Gpr156* mutants was only recapitulated using ptxA (**Figure 1C**) (Kindt et al, 2021). If ptxA-based orientation defects are physiologically relevant to GNAI function, they might be observed in *Gnai2; Gnai3* mutants as well. As mentioned above, a caveat to test this assumption is that highly dysmorphic hair bundles in *Gnai2; Gnai3* mutants obscure HC orientation.

To circumvent this limitation, we first excluded near-symmetrical HC in the *Gnai2; Gnai3* mutant datasets since an asymmetric cytoskeleton is pre-requisite for HC to exhibit a defined orientation (excluded: eccentricity<0.4 at E17.5 and <0.25 at P0). Next, we used the position of the off-center basal body to infer the orientation of the remaining asymmetric HC, ignoring the shape of the hair bundle. We measured the angle formed by a vector running from the HC center to the basal body relative to the cochlear longitudinal axis (α, see schematic in **Figure 8**). Angles were plotted in circular histograms where 0° points to the cochlear base and 90° to the lateral edge. At E17.5 at the cochlear mid position, *DIO-ptxA* showed the graded pattern of OHC misorientation observed as early as these cells break planar symmetry (Kindt et al, 2021), with inverted OHC1 and OHC2 and imprecisely oriented IHC and OHC3 (**Figure 8A**). *DIO-ptxA* OHC1-2 maintained this misorientation profile at the E17.5 base and at P0 (**Figure 8B-D**) as well as in adults (**Figure 2A**).

At the E17.5 cochlear mid, many but not all OHC1 were strikingly inverted as well in *Gnai2; Gnai3* mutants (**Figure 8A**). The majority of more mature OHC1 at the E17.5 cochlear base were inverted (**Figure 8B**), as were P0 OHC1 at all positions (**Figure 8C**- D; **Figure 8 Supp. 1A**). Loss of GNAI2 and GNAI3 can thus recapitulate inverted OHC1- 2 observed in the *DIO-ptxA* model with what appears to be a delay. In contrast however, OHC2 were generally oriented laterally (90°) at E17.5 and at the P0 apex and mid in *Gnai2; Gnai3* mutants (**Figure 8A-C**; **Figure 8 Supp. 1A**). OHC2 only adopted inverted orientation characteristic of the *DIO-ptxA* model at the P0 base where HC are more mature (**Figure 8D**). As OHC2 mature later than OHC1 (Anniko, 1983), this again suggests a delay where GPR156-GNAI signaling can initially reverse OHC1-2 normally, but where a lateral orientation cannot be maintained and OHC1-2 ultimately become inverted as in the *DIO-ptxA* model.

FoxG1-Cre is expressed at the otocyst stage in cochlear progenitors (Hebert & McConnell, 2000) and globally downregulates GNAI/O proteins early on in the *DIO-ptxA* model. However, *FoxG1-Cre*-mediated deletion at the *Gnai3* locus in *Foxg1-Cre*; $Gnai2^{del/del}$; $Gnai^{flox/flox}$ mutants might preserve some functional GNAI3 proteins for a longer time and explain the apparent delay in OHC1-2 misorientation. To test this idea, we delayed GNAI downregulation by ptxA and asked whether this would result in a milder, delayed OHC1-2 misorientation phenotype as seen in *Gnai2; Gnai3* mutants. For that goal, we used the *Atoh1-Cre* driver which is only active in postmitotic HC (Matei et al, 2005). Strikingly, while P0 OHC1 were inverted in *Atoh1-Cre; DIO-ptxA* as in *FoxG1-Cre; DIO-ptxA*, OHC2 generally pointed laterally (90°) in *Atoh1-Cre; DIO-ptxA* as in *Gnai2; Gnai3* mutants at the E17.5 base and the P0 apex (**Figure 8 Supp. 1B**). However, a large proportion of OHC2 were inverted at the P0 base, supporting the hypothesis of a delayed inversion following delayed GNAI loss-of-function.

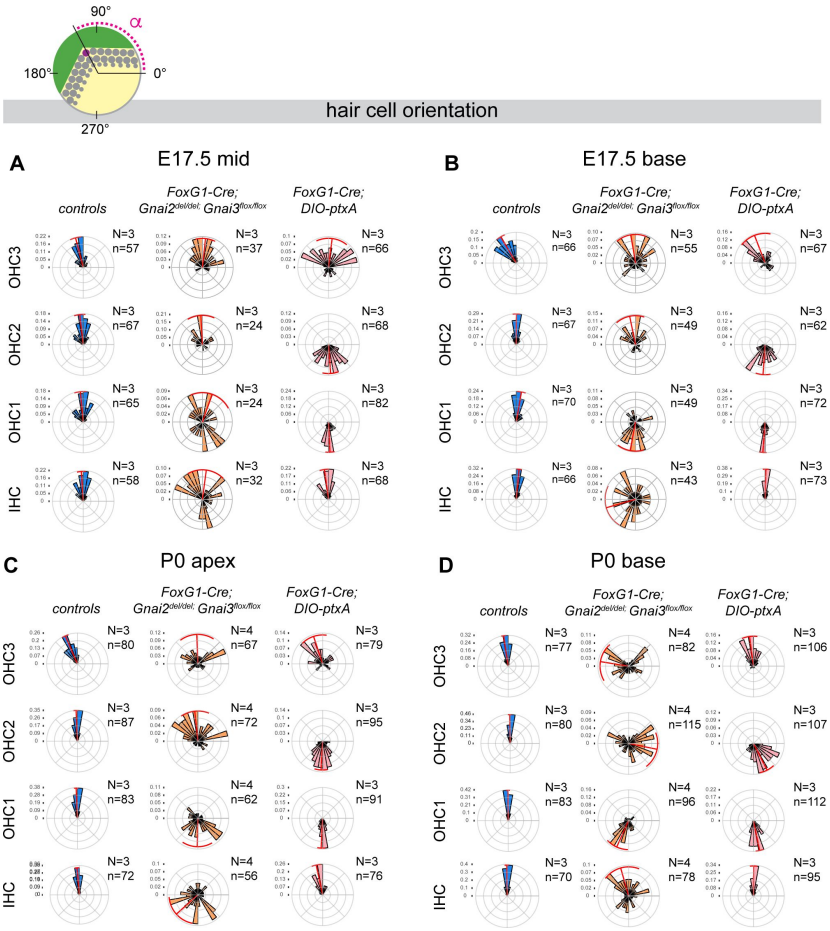

Figure 8.

Loss of GNAI2 and GNAI3 recapitulates hair cell orientation defects observed in *ptxA* mutants.

A-D) Circular histograms showing HC orientation (α) based on the position of the basal body (purple dot in top diagram) at the stage and cochlear position indicated. 0° is towards the cochlear base and 90° is lateral. HC represented have an eccentricity greater than 0.4 in A-B (E17.5), and 0.25 in C-D (P0) (see **Fig. 7**). Histograms show frequency distribution (10° bins) and red radial lines and arcs respectively indicate circular mean and circular mean deviation. In control cochleae, HC are tightly oriented laterally (90°) except for OHC3 that show a slight bias towards the cochlear apex (180°). As reported previously, ptxA expression inverts OHC1 and OHC2, and results in imprecise lateral orientation of OHC3. This phenotype is recapitulated in *Gnai2; Gnai3* double mutants with a delay (compare least mature E17.5 mid (A) and most mature P0 base (D)). IHC also show severe misorientation in *Gnai2; Gnai3* double mutants, unlike in *ptxA* mutants. n, HC number in N=3-4 animals. Controls for *FoxG1-Cre; Gnai2*$^{del/del}$*; Gnai3*$^{flox/flox}$ are *Gnai2*$^{del/+}$*; Gnai3*$^{flox/+}$, *Gnai2*$^{del/+}$*; Gnai3*$^{flox/flox}$, *FoxG1- Cre; Gnai2*$^{del/+}$*; Gnai3*$^{flox/+}$ and *FoxG1-Cre; Gnai2*$^{del/+}$*; Gnai3*$^{flox/flox}$. Data at the P0 cochlear mid position can be found in **Fig. 8 Supp. 1A**. Histograms for littermate controls of *FoxG1-Cre; DIO-ptxA* mutants can be found in **Fig. 8 Supp. 2**. Detailed cohorts and results can be found in Source Data file.

Together, these results first show that the *ptxA* misorientation pattern is present in *Gnai2; Gnai3* double mutants. Differences in severity between models can be explained by different timing of GNAI inactivation. Of note, the only surviving *Gnai2; Gnai3* double mutant we obtained suggests that OHC1-2 inversion is maintained in adults (**Figure 2A**), as in *ptxA* and *Gpr156* mutants (**Figure 2A**) (Kindt et al, 2021). Endogenous GNAI proteins are thus integral for OHC1-2 to reverse and adopt a proper lateral orientation during development, and at least transiently to maintain this lateral orientation. Second, these results also suggest that the GNAI activities required for symmetry-breaking, lateral HC orientation and for hair bundle morphogenesis are qualitatively different (**Figure 9**). *Gnai2; Gnai3* mutants are more severely affected considering symmetry-breaking and hair bundle morphogenesis, whereas *DIO-ptxA* mutants appear more severely affected considering OHC1-2 orientation. Of note however, IHC and OHC3 were severely misoriented in *Gnai2; Gnai3* mutants at all stages and positions analyzed, but much less affected in *DIO-ptxA* mutants (**Figure 8**; **Figure 8 Supp. 1A**). We discuss below how different GNAI protein identity, dose, timing and upstream regulators may underlie different roles (**Figure 9**) and explain differences in phenotype across mutant models.

Discussion

By examining a large collection of single and combined mutations in *Gnai/o* genes (*Gnai1*, *Gnai2*, *Gnai3*, *Gnao1*), we assign here three distinct roles for GNAI proteins during the apical polarization of a developing HC (**Figure 9**): a) to drive the centrifugal migration of the basal body when a prospective HC breaks planar symmetry and b) to orient this migration along the PCP axis in a binary manner, and c) to position and elongate stereocilia during hair bundle morphogenesis. Key results in the study include demonstrating that endogenous GNAI proteins indeed serve early functions (a) and (b), since to date only hair bundle defects (c) were reported in knock-out mouse models where *Gnai* genes were targeted (Beer-Hammer et al, 2018; Mauriac et al, 2017). Previous studies suggested that GNAI proteins partner with different regulators to fulfill different roles, organizing and elongating stereocilia by binding the scaffold GPSM2 (c), and reversing HC orientation in *Emx2*-expressing HC downstream of the receptor GPR156 (b).

Different GNAI/O identity, dosage and timing underlie different roles

Interestingly, besides involving different regulators, each role also appears to involve different dosage and specific identity of the underlying GNAI protein(s) at different times during HC development (**Figure 9**). For postnatal hair bundle morphogenesis (c), GNAI proteins are sequestered in the GDP-bound state by GPSM2, forming a complex highly enriched at the bare zone and at row 1 stereocilia tips that can be reliably immunodetected (Akturk et al, 2022; Kindt et al, 2021). In these two sub-cellular compartments, the identity of the GNAI proteins at work matters, with GNAI3 playing a required and prominent role while GNAI2 is important yet not required. Although one of our GNAI antibodies can detect GNAI1, we did not observe GNAI1 signals in HC (**Figure 4**), and *Gnai1* mutants did not exhibit significant hair bundle defects or ABR threshold shifts (**Figure 2**; **Figure 3A**). On the other hand, we observed a trend towards more severe stereocilia defects and more elevated ABR thresholds in *Gnai1; Gnai3* compared to single *Gnai3* mutants (**Figure 2C-E**; **Figure 3D**). Together, these results suggest that GNAI1 plays a minor, or no role in hair bundle development, with differences in the genetic background between strains possibly explaining the latter results. Similarly, we did not observe HC or auditory defects in absence of GNAO.

In stark contrast with its inability to rescue hair bundle morphogenesis (c), GNAI2 can fully rescue the off-center migration of the basal body (a) and its direction which defines HC orientation (b) when both GNAI1 and GNAI3 are constitutively absent. These two early roles are qualitatively different because they do not strictly reflect a difference in timing (a and b occur at the same time)

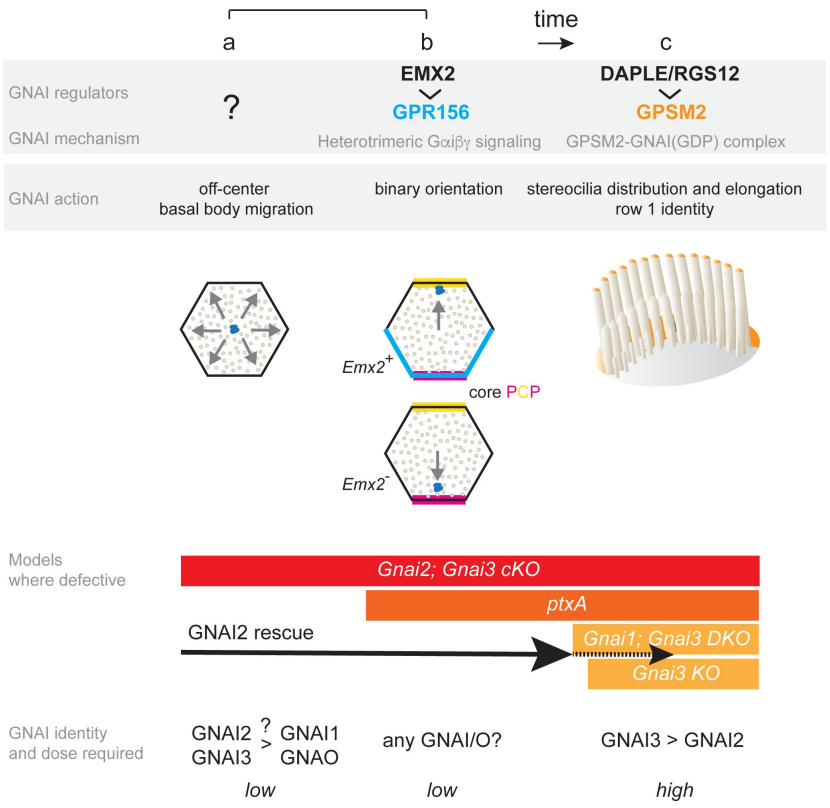

Figure 9.

Summary and model: three roles validated *in vivo* for GNAI proteins during hair cell polarized morphogenesis.

GNAI proteins are required for the off-center migration of the basal body, and thus HC symmetry breaking (a). This activity is distinct from defining binary HC orientation downstream of GPR156 (b), as *Gpr156* mutant HC have off-center basal bodies and normal hair bundles. Finally, GNAI partner with GPSM2 to shape the hair bundle and elongate stereocilia (c). The specific identity and the dosage of GNAI proteins required differ for each role. GNAI3 is the principal architect of hair bundle development (c), with GNAI2 plays an important but progressively waning role. High amounts of GNAI3/GNAI2 are required with GPSM2. A lower dose of GNAI/O proteins is required for embryonic role, and we speculate that GNAI2 and GNAI3 play a prominent role for symmetry-breaking (a) whereas any GNAI/O protein may effectively signal downstream of GPR156 for proper HC orientation (b). A GNAI/O regulator for symmetry breaking remains to be identified.

or GNAI/O dose. Symmetry-breaking (a) is affected in *Gnai2; Gnai3* double mutants but is intact in the *ptxA* model despite early (*FoxG1-Cre*) and high (caggs promoter) expression of untagged pertussis toxin. On the contrary, orientation of OHC1-2 (but not IHC and OHC3) is most severely affected in the *DIO-ptxA* model, with *Gnai2; Gnai3* mutants showing delayed defects. PtxA downregulates but does not abolish GNAI/O proteins, and we thus conclude that ptxA cannot achieve a loss of GNAI2 and GNAI3 function as extensive as in double targeted mutants. Among GNAI/O proteins, GNAI2 and GNAI3 may be more specifically required for HC to break symmetry, but other GNAI/O proteins and/or other factors may participate as well since a majority of HC eventually break symmetry even in *Gnai2; Gnai3* mutants. On the other hand, GPR156 is known to signal via heterotrimeric GNAI proteins (Watkins & Orlandi, 2021), and we speculate that any GNAI/O protein may equally relay signals to regulate HC orientation. PtxA would thus be a particularly effective way to disrupt the orientation role (b), with GNAI1 and/or GNAO partially rescuing orientation in *Gnai2; Gnai3* mutants. Our results also suggest that GNAI/O proteins are not only required for OHC1-2 to adopt a normal lateral instead of medial orientation upon symmetry-breaking (normal GPR156-driven reversal; **Figure 9**), but also to maintain this lateral orientation, at least transiently. Delayed GNAI/O inactivation indeed appears to result in initially normal OHC1-2 lateral orientation followed by a switch to medial orientation in a proportion of cells (abnormal inversion; **Figure 8**; **Figure 8 Supp. 1B**).

Regarding dosage, we propose that embryonic activities (a, b) run on low GNAI/O amounts compared to hair bundle functions (c). Of note, GNAI/O proteins are not immunodetected along with GPR156 in HC (b) but are easily detected with GPSM2 at the bare zone and stereocilia tips (Akturk et al, 2022; Kindt et al, 2021). This may be because GNAI/O proteins in heterotrimeric G protein complexes cycle dynamically between a GDP and GTP-bound state at low dose and escape immunodetection. In this context, it should be noted that a GNAI/O regulator for symmetry-breaking and its mode of action remain unknown (**Figure 9**, role a).

A time- and dosage-dependence for early GNAI roles can explain why our conditional *Gnai2; Gnai3* double mutant model is more severely affected than a comparable conditional *Gnai2; Gnai3* model where only hair bundle defects (c) were reported (Beer-Hammer et al, 2018). While Beer-Hammer and colleagues used *FoxG1-Cre* as a driver as we did, combined GNAI2 and GNAI3 inactivation necessitated Cre recombination at four floxed loci ($Gnai2^{flox/flox}$; $Gnai3^{flox/flox}$). In contrast, our model necessitates recombination at two loci only ($Gnai2^{del/del}$; $Gnai3^{flox/flox}$). We thus conclude that our model achieves an earlier and further loss of GNAI2/GNAI3 activity. This hypothesis is supported by extensive postnatal lethality in our model, whereas Beer-Hammer and colleagues could analyze *Gnai2; Gnai3* double mutants as adults. Our work thus usefully reconciles previous reports about GNAI functions in HC, notably showing that inactivating endogenous GNAI proteins does produce early defects (a,b) so far only observed with ptx. We thus validate all HC defects observed with ptx as physiologically relevant and specific to GNAI/O function.

Hair cell break of symmetry

Although cochlear HC expressing ptxA undergo normal symmetry-breaking in vivo (this work and (Kindt et al, 2021; Tadenev et al, 2019; Tarchini et al, 2013; Tarchini et al, 2016)), a fraction of utricular and saccular HC expressing myc:ptxA showed an abnormally central basal body (Kindt et al, 2021). This suggests that a higher dose of GNAI/O is required for the off-center migration of the basal body in vestibular compared to cochlear HC, making vestibular HC more susceptible to ptxA. “Ciliary” proteins are required for ciliogenesis, including kinocilium formation and maintenance, and also play non-ciliary functions (May-Simera et al, 2015; Sipe & Lu, 2011). Inactivation of intraflagellar transport protein IFT88 was reported to result in a central basal body and circular hair bundles in ~10% of OHC (Jones et al, 2008), but the underlying mechanism was not elucidated. A low proportion of symmetrical HC was also reported in absence of the CD2 isoform of the protocadherin PCDH15 that forms inter-stereocilia and kinocilium-stereocilia

fibrous links during embryogenesis (Webb et al, 2011). It remains unclear whether GNAI/O activity participates in *Ift88* or *Pcdh15* mutant defects, or whether GNAI could be active at the basal body or the kinocilium.

Hair cell orientation

The planar cell polarity (PCP) axis is defined by opposite asymmetric enrichment of the core PCP transmembrane proteins VANGL2 and FZD3/6 and their specific cytosolic partners at the apical junction of HC and support cells (Deans, 2013; Montcouquiol & Kelley, 2019; Tarchini & Lu, 2019). Previous work showed that regional *Emx2* expression reverses how the HC basal body migrates relative to uniform and early-set core PCP landmarks, notably establishing the line of polarity reversal in the utricle and saccule. EMX2 activates the GPR156 receptor by triggering its polarized enrichment at the apical HC junction, where downstream GNAI/O signaling appears to reverse how core PCP cues are interpreted and to repel the basal body (**Figure 9**, role b) (Kindt et al, 2021). EMX2 achieves this goal by preventing expression of the kinase STK32A that suppresses apical enrichment and polarization of the GPR156 protein (Jia et al, 2023). It is important to note that HC lacking GPR156 have a normal apical cytoskeleton, including a normally formed hair bundle, and only show orientation defects (Kindt et al, 2021). This indicates that the centrifugal migration of the basal body and the direction of this migration that defines early HC orientation are two distinct molecular mechanisms although both involve GNAI/O proteins (**Figure 9**; a *versus* b). Similarly, HC lacking GPSM2 are not inverted in orientation as in *Emx2*, *Gpr156*, *Gnai2; Gnai3* or *ptxA* mutants (Bhonker et al, 2016; Ezan et al, 2013; Tarchini et al, 2013). This indicates that bare zone enrichment of the GPSM2- GNAI complex is a mechanism to shape and polarize the growth of the hair bundle, but not to migrate off-center or orient the basal body. GPSM2-GNAI is polarized on the side of the off-center basal body but occupies the HC apical membrane and not the apical junction where core PCP proteins regulate HC orientation (Siletti et al, 2017; Tarchini et al, 2013).

While both GPR156 (Greene et al, 2023; Ramzan et al, 2023) and GPSM2 (Doherty et al, 2012; Walsh et al, 2010) have been identified as human deafness genes, there is currently no evidence implicating a GNAI/O protein. This is most likely because all GNAI/O proteins, including GNAI3 which is more specifically required in HC for hair bundle morphogenesis (**Figure 9**), play ubiquitous and critical signaling roles in the context of heterotrimeric protein signaling across many cell types.

Methods

Mouse strains and husbandry

All mouse strains used in this work and strain-related information is summarized in Supplementary Table 1. All primers used for genotyping are indicated in Supplementary Table 2 by strain.

Strains from The Jackson Laboratory repository

Gnai1^{neo}*; Gnai3*^{neo} (*Gnai1*^{tm1Lbi}*; Gna3*^{tm1Lbi}; MGI: 5560183) (Jiang et al, 2002) carries a neo cassette in *Gnai1* exon 3 and a neo cassette replacing part of intron 5 and exon 6 in *Gnai3* in the 129S1/SvlmJ background. The single *Gnai1*^{neo}and single *Gnai3*^{neo} alleles were segregated from *Gnai1*^{neo}*; Gnai3*^{neo} by breeding with C57BL/6J mice and are consequently on a mixed 129S1/SvlmJ: C57BL/6J background. *Gnao1*^{neo} (*Gnao1*^{tm1Lbi}; MGI: 2152685) carries a neo cassette in *Gnao1* exon 6 in the 129S1/SvImJ background (Jiang et al, 2002). The two *Cre* strains used in this work are *Atoh1-Cre* (*Tg(Atoh1-cre)1Bfri;* MGI: 3775845) expressing Cre in HC from E14.5 (Matei et al, 2005) and *FoxG1-Cre* (*Foxg1*$^{tm1(cre)Skm}$; MGI: 1932522) expressing Cre in the prospective otic vesicle from E8.5 (Hebert & McConnell, 2000).

Consortium strain

Gnao1^{flox} (*Gnao1*$^{tm1c(EUCOMM)Hmgu}$) was derived from the EUCOMM strain *Gnao1*$^{tm1a(EUCOMM)Hmgu}$ (MGI: 4456727; "KO first, conditional ready"). The *Gnao1*^{flox}conditional allele was produced via FLP-mediated recombination (FLP strain MGI: 4830363) to remove the FRT-flanked *LacZ-neo* cassette, leaving exon 3 floxed. *Gnao1*^{flox} is on C57BL/6N background.

Constitutive *Gnai2*^{del} inactivation (see **Figure 2 Supp. 1A**).

Gnai2^{del} (*Gnai2*$^{em1Btar;}$ MGI: 6466534) was generated using delivery of CRISPR-Cas9 reagents in mouse zygotes via electroporation. The following guide RNAs (gRNAs) were used to delete exon 2, exon 3 and part of exon 4 in the C57BL/6J background. Upstream gRNA: CTGCCCTCTGTTCCAGGTGC, downstream gRNA: ATGCTTCCTGAAGACCTGTC. The resulting 681 bp deletion encompassed TGCTGGAGAGTCAGGGAAGA…CCTGAAGACCTGTCCGGTGT. The electroporation mixture consisted of the gRNAs with AltR- *Streptococcus pyogenes* Cas9 (SpCas9) V3 (Integrated DNA Technologies #1081059) in embryo-tested TE buffer (pH 7.5). Electroporation of zygotes was performed as described in (Qin et al, 2015). In order to segregate away potential non-specific mutations, founders were bred for two generations with C57BL/6J animals to generate a N2 heterozygote stock. Because *Gnai2*^{del} homozygotes showed low viability, this strain was used in a mixed C57BL/6J:FVB/J background that improved the proportion of homozygotes (see **Supp. Table 1**).

Conditional *Gnai3*^{flox} inactivation

(see **Figure 2 Supp. 1B**). A plasmid-based donor vector was cloned to flank *Gnai3* exon 2 and 3 with *loxP* sites using the same CRISPR/Cas9 system as described above for *Gnai2*$^{del.}$A fragment carrying a *loxP*, a genomic region including exon 2-3, the restriction site ClaI, a second *loxP* and the restriction site XhoI was synthetized (Genscript) and cloned between 5' and 3' homology arms amplified by PCR using Gibson assembly. The following gRNAs were used and define the extremities of the floxed region: upstream, AGCTCACCAAAATTCCCATT, TAGGGGATATAGATCCAAAT, downstream, TTCCAGGACTCTGCATGCGT, TACCGACGCATGCAGAGTCC. The gene editing reagents (gRNAs, donor vector, SpCas9) were microinjected in zygotes as described in (Qin et al, 2015). To confirm insertion at the *Gnai3* locus, we performed long-range PCRs with a genomic primer located outside the homology arm on each side: *5' long-range:* F(external)_ TACTGAGATGAGAGACTGAGGG and R (internal)_TGGCTGACATCCTTTGATGGAC. The 3070 bp product was digested with XhoI, producing 2,551 + 519 bp fragments upon donor insertion (flox allele). 3' long-range: F (internal)_TGAAAGGTAAAGGCAACGTGAG and R (external)_TGTGAGACAGGGTCTCTCTTTG. The 2,966 bp product was digested with XhoI, producing 2,000 + 966 bp fragments upon donor insertion (flox allele). In order to segregate away potential non-specific mutations, founders were bred for two generations with C57BL/6J animals to generate a N2 heterozygote stock.

Pertussis toxin catalytic subunit (ptxA)-expressing strains

(see **Figure 2 Supp. 1C-D**). The *LSL-myc:ptxA* strain at the *ROSA26* (*R26*) locus was described previously (*Gt(ROSA)26Sor*$^{em1(ptxA)Btar}$; MGI: 6163665) (Tarchini et al, 2016). The new *CAG-DIO-ptxA* strain line (see **Figure 2 Supp. 1D**) was generated at the *R26* locus using the Bxb1 attP(GT) integrase technology and *C57BL/6J-Gt(ROSA)26Sor*$^{/Mvw}$(MGI: 6757188) as the host strain (Low et al, 2022). The donor vector consisted in a CAG promoter followed by the flipped ptxA coding sequence flanked by double inverted lox sites (loxP and lox2272; **Figure 2 Supp. 1D**) and a bGHpA sequence. In order to exclude the prokaryotic vector backbone, the donor vector was prepared as a minicircle using the MC-Easy Minicircle Production kit (SystemBio, MN920A-1). Briefly, the donor plasmid insert was cloned into a Minicircle Cloning Vector using PhiC31 integrase before transformation into the ZYCY10P3S2T *E. coli* minicircle producer strain, which

after induction with arabinose, results in the generation of the donor minicircle. To eliminate parental plasmid contamination, a restriction digest was performed, followed by MC-safe DNase treatment. The minicircle DNA was then purified by phenol-chloroform extraction and reconstituted in microinjection buffer (10 mM Tris; 0.1 mM EDTA pH7.5). The *CAG- DIO-ptxA* strain was generated by pronuclear microinjection of the Bxb1 Integration reagents directly into zygotes of the host strain. These reagents included the Bxb1 mRNA (Trilink) at 100ng/µl, RNasin (Promega) at 0.2U/µl and the donor minicircle DNA at 10ng/µl combined in microinjection buffer. To confirm successful integration of the 3,212bp transgene, as well as identify random transgenics, the initial screening was performed using a four-PCR strategy. The In/Out Left and Right (IOL, IOR) PCRs, which bridge the recombined attachment sites, each contain one primer specific to the *R26* locus and a second primer designed against the inserted sequence. The Transgene (TG) PCR amplifies a non-genomic sequence in the insert, and the Off-Target Integration (OTI) PCR was designed to detect non-recombined minicircle integration, presumably outside of the *R26* locus.

IOL PCR (F1/R1), F1: GTCGCTCTGAGTTGTTATCAGT, R1: GCCAAGTAGGAAAGTCCCATAA (720 bp, WT=no band). IOR PCR (F2/R2), F2: GGTGATGCCGTTGTGATAGA, R2: TGTGGGAAGTCTTGTCCCTCCAAT (1,013 bp, WT=no band). TG PCR (F2/R3) F2: 5'-GGTGATGCCGTTGTGATAGA, R3: CCACTTCATCGGCTACATCTAC (214 bp, WT=no band). OTI PCR (F3/R1) F3: GGGAGGATTGGGAAGACAATAG, R1: GCCAAGTAGGAAAGTCCCATAA (578 bp, WT=no band). 33 mice were born following 6 transfers totaling 117 injected embryos (28% survival), and 1/33 (3%) was identified as a founder and crossed to C57BL6/J to generate N1 offspring. The In/Out PCR confirmed that a copy of the transgene was inserted at the *R26* locus, but the OTI strategy also gave a product, even after breeding for multiple generations. As breeding would have segregated a separate, random integration of the transgene, we performed Nanopore-based Cas9-targeted sequencing at the *R26* locus (Gilpatrick et al, 2020; Low et al, 2022). This revealed that, as seen in some cases previously (Low et al, 2022), tandem insertion had occurred in this founder Specifically, 3 consecutive copies of the *CAG-DIO-ptxA* transgene were inserted at the *R26* locus in this strain. This did not impact specific Cre-based expression of ptxA because phenotypes observed in this new strain were comparable to the previous *LSL- myc:ptxA* strain (**Figure 6** Supp.1 B-D).

Experimental animals in the study ranged in age between E17.5 and P29 as indicated in each figure. Male and females were systematically included but sex was not tracked except for Auditory Brainstem Recordings because there is no evidence that sex influences HC orientation or hair bundle morphogenesis. Animals were maintained under standard housing conditions (14h light / 10h dark cycle, ambient temperature and normal humidity). All animal work was reviewed for compliance and approved by the Animal Care and Use Committee of The Jackson Laboratory (Animal Use Summary AUS #14012).

Scanning Electron Microscopy

(SEM) Temporal bones were isolated, punctured at the cochlear apex, and fixed by immersion for at least one overnight at 4°C in 2.5% glutaraldehyde (Electron Microscopy Sciences; 16200) and 4% paraformaldehyde (Electron Microscopy Sciences; 15710) in 1mM MgCl2, 0.1M Sodium Cacodylate, 20mM CaCl2. Samples were rinsed and decalcified overnight in 4% EDTA. The auditory epithelium was then dissected into 3 pieces (cochlear base, mid, and apex) before progressive dehydration in an ethanol series (30-50-70-80-90- 100%, at least 20 minutes per step) and chemical drying with hexamethyldisilazane (HMDS; Electron Microscopy Sciences 50-243-18). Dry samples were mounted on aluminum stubs using double-sided carbon tape and sputter-coated with gold-palladium before imaging on a Hitachi 3000N VP electronic microscope at 20kV.

Immunofluorescence and antibodies

For embryonic and postnatal stages, temporal bones were immediately dissected to expose the sensory epithelium and fixed in paraformaldehyde (PFA 4%; Electron Microscopy Sciences; 15710) for 1h at 4°C. After fixation, the tectorial membrane was removed, and samples were

permeabilized and blocked in PBS with 0.5% Triton-X100 and bovine serum albumin (1%) for at least at 1 hour at room temperature. For adult stages, temporal bones were isolated and punctured at the cochlear apex to facilitate access of the fixative. Samples were then immersion-fixed in PFA 4% for 1 hour at 4°C, rinsed in PBS, and incubated overnight in 4% EDTA for decalcification. Cochleae were next dissected in 3 pieces (cochlear base, mid, and apex), before permeabilization and blocking as described above. Primary and secondary antibodies were incubated overnight at 4°C in PBS with 0.025% sodium azide. Fluorescent dye-conjugated phalloidin was added to secondary antibodies. Samples were washed 3 times in PBS + 0.05% Triton-X100 after each antibody incubation and post-fixed in PFA 4% for at least 1 hour at room temperature. Samples were then mounted flat on microscopy slides (Denville M102) using Mowiol as mounting medium (Calbiochem/MilliporeSigma 4759041), either directly under a 18×18mm #1.5 coverglass (VWR 48366-045) (postnatal cochleae) or using one layer of office tape as a spacer (adult cochleae). Mowiol (10% w/v) was prepared in 25%(w/v) glycerol and 0.1M Tris-Cl pH8.5. Primary antibodies used were:

Rabbit anti-GNAI2, pt"GNAI2" (Proteintech, 11136-1-AP); the antigen is the full human GNAI2 protein

Rabbit anti-GNAI3, scbt"GNAI3" (Santa Cruz Biotechnology, sc-262); the antigen is undisclosed but corresponds to a C-terminal region of the rat GNAI3 protein

Rabbit anti-GNAO (Proteintech, 12635-1-AP)

Mouse anti-acetylated alpha tubulin (Santa Cruz Biotechnology scbt-23950)

Rabbit anti-GPSM2 (Sigma, A41537)

Goat anti-GPSM2 (Thermofisher, PA5-18646)

Rabbit anti-Pericentrin/PCNT (Biolegend/Covance, PRB-432C)

Rat anti-ZO1 (Developmental Studies Hybridoma Bank, R26.4C)

Secondary antibodies from ThermoFisher Scientific were raised in donkey and conjugated to Alexa Fluor (AF) 488, 555, or 647 (donkey anti-rabbit AF555 (A-31572), AF647 (A-31573), donkey anti-mouse AF647 (A-31571), donkey anti-rat AF488 (A- 21208), donkey anti-goat AF555 (A-21432), AF647 (A-21447)). Fluorescent conjugated phalloidins used to reveal F-actin were from ThermoFisher Scientific (AF488 (A12379); AF555 (A34005)) and Sigma-Aldrich (FITC (P5282)).

Inner ear electroporation and cochlear culture

Inner ears from wild-type animals (mixed C57BL/6J-FVB/NJ background) were harvested at E13.5 in HBSS/5mM Hepes. Caggs plasmid vectors (CMV early enhancer, beta-actin promoter) driving either mouse *Gnai1*, *Gnai2* or *Gnai3* cDNA expression were mixed with Fast Green FCF (0.05%; Sigma, F7252) and injected at 2.5mg/ml in the cochlear duct using a Wiretroll capillary and plunger (Drummond, 53507-426). Injected inner ears were next electroporated (BTX ECM830; 27V, 27 ms, 6 square pulses at 950 ms intervals), the condensed mesenchyme was dissected away and the soft cochlear labyrinth was embedded in 50% Matrigel (Corning, CB40234). Cochlear explants were cultured for 6 days in DMEM with 10% fetal bovine serum and 10 µg/ml ciprofloxacin (Sigma, 17850). Explants were then fixed in 4% PFA for 15 min at room temperature before being processed for immunolabeling.

Sample cohorts, image acquisition and analysis

All quantifications include at least three animals per genotype. All graphs or their legends indicate the animal cohort size (N) as well as the number of HC or stereocilia (n) analyzed. Further details can be found in the Supplementary Source Data file where tabs are referencing figure panels in order. When an experimental outcome was not quantified, at least 3 mutant and 3 control littermates encompassing two or more litters were analyzed, and figure panels illustrate a representative outcome observed in all samples of the same genotype. A single exception is adult *Foxg1-Cre; Gnai2*$^{del/del}$*; Gnai3*$^{flox/flox}$ data in **Fig. 2A**- F where a single mutant animal was analyzed since we failed to obtain others at 3 weeks of age in spite of extensive breeding (see **Supp. Table 1**).

Confocal images were captured with a LSM800 line scanning confocal microscope, a 63x NA1.4 oil objective, the Airyscan detector in confocal mode (except in **Figure 5** Supp.1 D, E where the Airyscan detector was used in Airyscan mode) and the Zen 2.3 or Zen 2.6 software (Carl Zeiss AG). Raw Airyscan images in **Figure 5** Supp.1 D, E were processed in Zen 2.6 selecting for automatic strength. Unless stated otherwise in the legends, images show a single optical z plane. To quantify HC eccentricity (**Figure 7**), images were captured with a Leica DM5500B widefield microscope, a 63x oil objective, a Hamamatsu ORCA-Flash4.0 sCMOS camera and the Leica Application Suite (LasX) software (Leica Microsystems). All confocal images in the same experiment were acquired using the same laser intensity and gain, and were then processed in Adobe Photoshop (CC2020) where the same image treatment was applied across conditions.

To measure stereocilia length and width in IHC (**Figure 2C-D**), SEM samples were imaged laterally at 10,000x magnification and with an appropriate tilt (from 0 to 30°) to bring stereocilia parallel to the imaging plane and minimize parallax. To quantify the number of rows in adult IHC and the number of stereocilia in their first row (**Figure 2E**, F), SEM samples were imaged medially at 5,000x magnification. To measure the length of OHC hair bundle wings (**Figure 2G**, **Figure 2 Supp. 1E**), OHC were imaged top down at 5,000x. Stereocilia width was measure at half-length and all measurements were done with the straight-line tool in Fiji.

To quantify GNAI signal intensity in *Gnai1*^{neo}*; Gnai3*^{neo} mutants (**Figure 5C**, **Figure 5 Supp. 1A**), Z-stack series were acquired at the mid cochlear position. A single Z slice was chosen at the bare zone level, another one at the stereocilia tip level, each based on strongest signal in that compartment. The vertex of the V-shaped hair bundle was used to divide the HC apical surface in two equal halves. In each half (left and right), regions of interest (ROIs) were drawn using the polygon selection tool in Fiji to encompass all signals in that apical compartment, and mean gray values were measured. For each image, background signal was measured and averaged, and subtracted from all measurements in the same image.

To quantify surface area of the bare zone or total surface area in half-OHC as well as the length of half hair bundles (**Figure 5G**, **Figure 5 Supp. 1C**; **Figure 6D**, H), Z-stack series were acquired at the cochlear base and a single Z slice was selected at apical junction level using ZO1 (**Figure 5G**, **Figure 5 Supp. 1C**) or F-actin (**Figure 6D**, H) as reference. To measure total apical surface area and bundle length in half-OHC, the pericentrin-stained basal body was used to divide the apical surface in two halves (**Figure 5G**, **Figure 5 Supp. 1C**). The ZO1-positive cell outline along with the dividing line at the basal body level were used as reference to measure surface area with the polygon selection tool in Fiji. To quantify the bare zone surface area (**Figure 6D**, H), a ROI was drawn around the total apical surface lacking phalloidin (F-actin) signals. The length of the F-actin stained hair bundle was measured using the straight-line tool in Fiji.

To determine HC eccentricity (**Figure 7**), the geometrical center of the HC apical surface was determined as the intersection of two orthogonal lines representing the maximal diameter of the cell along the cochlear longitudinal and radial axes. A vector (BB) was drawn from the center to

the pericentrin-labeled basal body, and eccentricity was calculated as the ratio of BB length over the cell radius (r) along the same trajectory using F-actin-labeled apical junction as landmark (see **Figure 7**). To determine cell orientation (**Figure 8** and **Figure 8 Supp. 1-2**), the angle (α) separating the longitudinal axis of the organ of Corti from the BB vector was measured with the angle tool in Fiji (see **Figure 8**). Both right and left cochleae were used and angles were measured so that 0° pointed toward the cochlear base and 90° towards the cochlear periphery (lateral). Eccentricity and angles were measured at the cochlear positions indicated (base ~20%, mid ~50%, apex ~80% of the cochlear length starting from the base).

Auditory Brainstem Response (ABR) tests

All tests were performed in a sound-attenuating chamber, and body temperature of the anesthetized animals was maintained at 37°C using a heating pad (FHC Inc.). Animals from all strains except *Atoh1-Cre; Gnao1*^{flox} (**Figure 3 Supp. 1B**, see below) were anesthetized with a mix of ketamine and xylazine (1 mg and 0.8 mg per 10g of body weight, respectively) and tested using the RZ6 Multi-I/O Processor System coupled to the RA4PA 4-channel Medusa Amplifier (Tucker-Davis Technologies). ABRs were recorded after binaural stimulation in an open field by tone bursts at 8, 16, 32, and in some cases 40 kHz generated at 21 stimuli/second, and a waveform for each frequency/dB level was produced by averaging the responses from 512 stimuli. Subdermal needles were used as electrodes, the active electrode inserted at the cranial vertex, the reference electrode under the left ear and the ground electrode at the right thigh.

Atoh1-Cre; Gnao1^{flox} animals (**Figure 3 Supp. 1B**) were anesthetized with tribromoethanol (2.5mg per 10g of body weight) and tested with the Smart EP evoked potential system from Intelligent Hearing Systems (IHS). ABR were recorded after single ear stimulation (right ear), using ear tubes speakers (ER3C insert earphones, IHS) delivering tone bursts at 8, 16, and 32 kHz generated at 40 stimuli/second. Electrodes were positioned as previously described except for the ground electrode that was placed at the base of the tail. ABR thresholds were obtained for each frequency by reducing the sound pressure level (SPL) by 5 decibels (dB) between 90 and 20 dB to identify the lowest level at which an ABR waveform could be recognized. We compared waveforms by simultaneously displaying 3 or more dB levels on screen at the same time.

Statistical Analyses

All data were plotted in Prism 9 (GraphPad), except for circular diagrams of HC orientation (**Figure 8**; **Figure 8 Supp. 1-2**) that were generated with R (4.2.2) and Rstudio (2022.12.0+353).

All data except for angles in circular diagrams (**Figure 8** and **Figure 8 Supp. 1-2**) were plotted individually. Distribution was framed with 25-75% whisker boxes where exterior lines show the minimum and maximum, the middle line represents the median, and + represents the mean. Potential differences in data distribution between genotypes were tested for significance using nested (hierarchical) t-test except for ABR thresholds (**Figure 3** and **Figure 3 Supp. 1**) where a 2-way ANOVA with Sidak's multiple comparison post-hoc test was used. Nested t-tests help avoid pseudoreplication by taking into consideration the data structure, here specifically variance in each animal (Eisner, 2021; Krey et al, 2023). OHC half-bundle lengths (**Figure 2G**, **Figure 2 Supp. 1E**) were plotted as paired left and right values in the same HC and a potential difference in data variance between genotypes was tested using a F-test. GNAI signal intensity at the OHC bare zone and stereocilia tips (**Figure 5C**, **Figure 5 Supp. 1A**) as well as OHC surface area and half-bundle length (**Figure 5G**, **Figure 5 Supp. 1C**) were plotted and a simple linear regression curve was calculated and drawn for each pair of datasets. A correlation between variables was addressed with Pearson's correlation test. Exact p-values were indicated on each graph when non-significant ($p>0.05$) and otherwise summarized as follows: $p<0.0001$ ****, $p<0.001$ ***, $p<0.01$**, $p<0.05$*. Details of statistical results for all figures can be found in the Supplementary Data file.

Angle frequency distribution (**Figure 8** and **Figure 8 Supp. 1**-**2**) was plotted in circular diagrams using the R package dyplr and the coord_polar function of the ggplot2 package to organize data and produce the graphs, respectively. The angle formed by the red line indicates the circular mean and the length of the arc at the end of the red line indicates the mean circular deviation. Both values were obtained using the colstats function in the R circular package. All scripts used in this work will be posted on github.

Acknowledgements

We are grateful to Elli Hartig for reading and commenting on the manuscript. We thank Simon Lesbirel for nanopore-based Cas9-targeted sequencing of the *DIO-ptxA* strain. We are grateful to The Jackson Laboratory Genome Engineering Technology and Reproductive Science services for their help with generating the $Gnai2^{del}$ and $Gnai3^{flox}$ strains, and cryorecovering the $Gnai1^{neo}$; $Gnai3^{neo}$and $Gnao1^{neo}$ strains, respectively. A.J. was supported by a postdoctoral fellowship from Fondation Pour l'Audition (2018-2020; FPA RD-2018-3). This work was supported by the National Institute on Deafness and Other Communication Disorders grants R01DC015242 and R01DC018304 (to B.T.).

Author contribution

B.T. conceived the study. B.T., A.J and A.L.T designed, performed and analyzed experiments. M.D. provided technical help with mouse colony maintenance, sample processing and genotyping. B. K. wrote the R script to generate the circular histograms. B.E.L and M.V.W. helped generate the *DIO-ptxA* strain using BxB1 recombination technology. B.T supervised the work. B.T. and A.J. wrote the manuscript. B.T. secured funding.

Competeting interests

The authors declare no competing interest.

Data availability

The data in all graphical representations are included in a single Source Data file. Original material used for quantifications and to build figures will be deposited in a publicly accessible repository.

References

Akturk A., Day M., Tarchini B (2022) **RGS12 polarizes the GPSM2-GNAI complex to organize and elongate stereocilia in sensory hair cells** *Sci Adv* **8**

Anniko M (1983) **Postnatal maturation of cochlear sensory hairs in the mouse** *Anat Embryol (Berl* **166**:355–68

Beer-Hammer S. *et al.* (2018) **Galphai Proteins are Indispensable for Hearing** *Cell Physiol Biochem* **47**:1509–1532

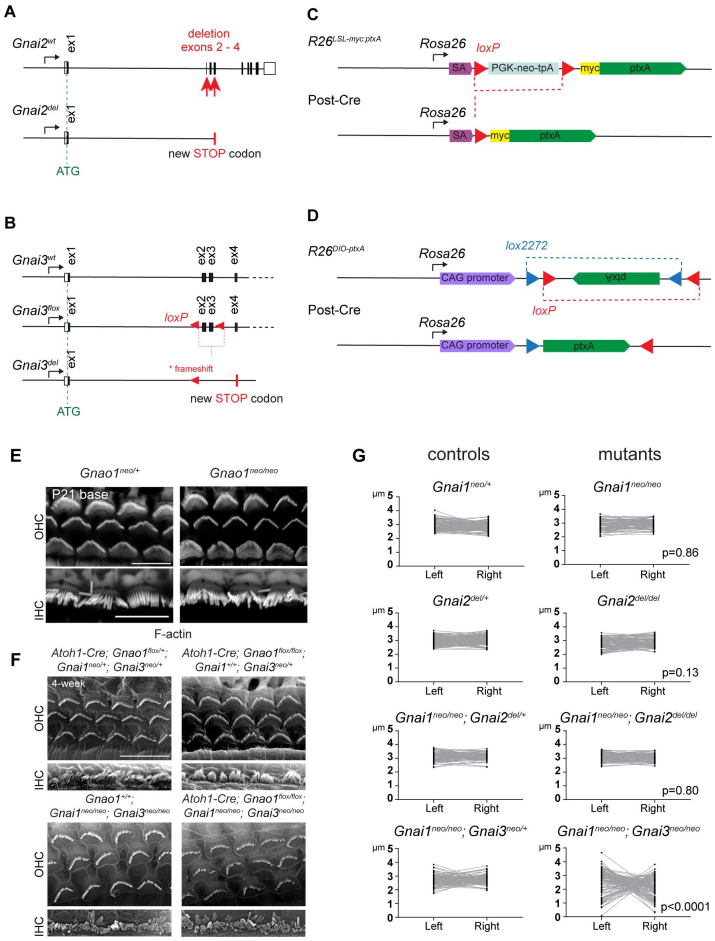

Figure 2 Supplement 1.

A-D) New mouse strains generated in this study are *Gnai2*^{del} (A), *Gnai3*^{flox} (B) and *R26*$^{DIO\text{-}ptxA}$ (D; see Methods for details). *R26*$^{LSL\text{-}myc:ptxA}$ was published previously and is used in this study as well (C). **E-F)** Loss of GNAO has no obvious impact on apical HC morphology or HC orientation. Representative confocal images of phalloidin-stained *Gnao1* constitutive mutants at P21 (E; *Gnao1*^{neo}) and scanning electron microscopy images of conditional *Gnao1* inactivation in the *Gnai1; Gnai3* double mutant background (F; *Gnao1*^{flox}). In F, top panels compare control (left) and conditional *Gnao1* inactivation (right) when GNAI1 and GNAI3 function is preserved. Bottom panels compare control (left) and conditional *Gnao1* inactivation (right) when GNAI1 and GNAI3 are inactivated. Note how HC-specific inactivation of GNAO using the *Atoh1-Cre* driver does not obviously enhance defects observed in *Gnai1; Gnai3* double mutants (F, bottom). **G)** Graphs showing the length of the left and right wing of 3-week-old OHC hair bundles paired by cell. Graphs for control littermates that were omitted in **Fig. 2G** are added here (left) next to repeated mutant graphs (right). p-values are for a F-test of variance of pooled left and right wing lengths compared to littermate controls. At least 3 animals and 88 OHC are represented per genotype. Only *Gnai3*^{neo} (**Fig. 2G**) and *Gnai1*^{neo}; *Gnai3*^{neo} mutants show truncated hair bundles and a significant p value (p<0.05).

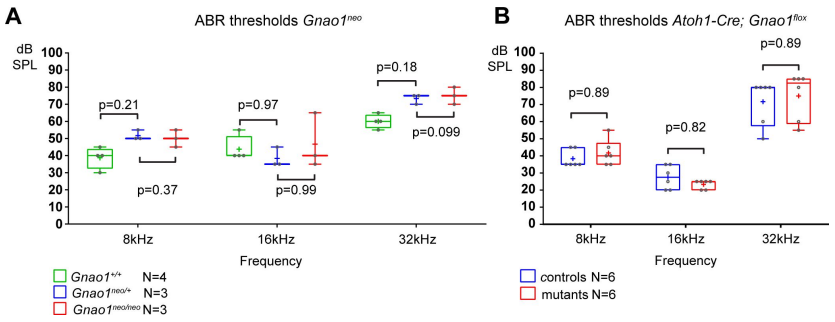

Figure 3 Supplement 1.

A-B) ABR thresholds at 8, 16, 32 kHz for constitutive *Gnao1* (A) and conditional *Atoh1-Cre; Gnao1*$^{flox/flox}$ (B) mutants tested between P20 and P25. Boxplots are framed with 25-75% whisker boxes where exterior lines show the minimum and maximum values, the middle line represents the median, and + represent the mean. N indicates the number of animals tested. In (B), because the original animal cohort was established to test whether the loss of GNAO could enhance defects in *Gnai1; Gnai3* double mutants (see **Fig. 2 Supp. 1F**), controls include the following genotypes: *Atoh1-Cre; Gnao1*$^{flox/+}$, *Gnao1*$^{flox/flox}$, *Gnai1*$^{neo/+}$*; Gnai3*$^{neo/+}$, *Gnai1*$^{neo/+}$, *Atoh1-Cre; Gnao1*$^{flox/+}$*; Gnai1*$^{neo/neo}$*; Gnai3*$^{neo/+}$ and *Gnai1*$^{neo/neo}$*; Gnai3*$^{neo/+}$ where other alleles are wild-type. Mutants include the following: *Atoh1-Cre; Gnao1*$^{flox/flox}$*; Gnai3*$^{neo/+}$ and *Atoh1-Cre; Gnao1*$^{flox/flox}$*; Gnai1*$^{neo/neo}$*; Gnai3*$^{neo/+}$ where other alleles are wild-type. Cohort details can be found in Source Data file. Two-way ANOVA with Sidak's multiple comparison. non-significant p-values are indicated. kHz, kiloHertz, dB SPL, decibel sound pressure level.

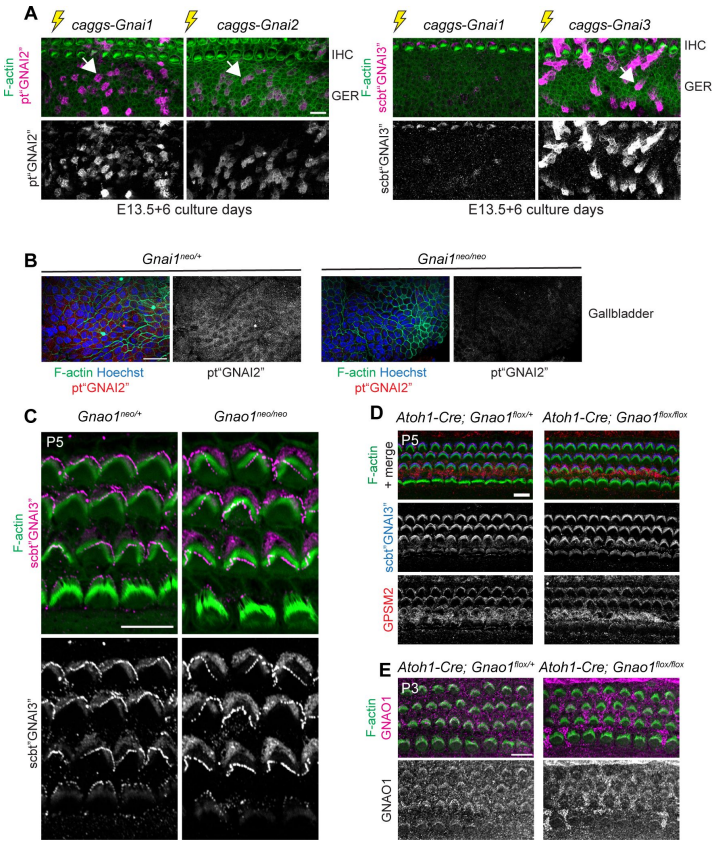

Figure 4 Supplement 1.

GNAI1 detection by Proteintech GNAI2 antibody, GNAI protein distribution in *Gnao1* mutants and lack of evidence for GNAO enrichment at the hair cell apex.

A) Cochlear explants electroporated at E13.5 with the Gnai constructs indicated and cultured for 6 days before immunolabeling with Proteintech (pt"GNAI2"; left) or Santa Cruz Biotechnology (scbt"GNAI3"; right) GNAI antibodies (maximum projections). pt"GNAI2" efficiently detects ectopically expressed GNAI1 (and GNAI2, as expected), but scbt"GNAI3" only weakly detects GNAI1 (and efficiently detects GNAI3, as expected). The greater epithelial ridge (GER) is imaged with IHC on top. Caggs: CMV early enhancer/beta-actin promoter expression vector. Results are representative of 3 independent explants.
B) pt"GNAI2" immunolabeling of the adult gallbladder epithelium (maximum projection) where specific *Gnai1* expression was reported in the *Gnai1*$^{tm1a(EUCOMM)Wtsi}$ mouse strain (International Mouse Phenotyping Consortium; *mousephenotype.org*). Apical signals are reduced in *Gnai1* mutants, confirming that the pt"GNAI2" antibody can detect endogenous GNAI1. **C-D)** GNAI (scbt"GNAI3" antibody; see **Fig. 4**) immunolabeling in P5 *Gnao1* constitutive (C) and *Atoh1-Cre; Gnao1*^{flox} conditional (D) mutants at the cochlear base. Enrichment of GNAI (C-D) and GPSM2 (D) at the bare zone and stereocilia tips is unchanged in absence of GNAO. **E)** GNAO immunolabeling at the P3 cochlear mid produces signals that are unspecific since they are unchanged in conditional *Gnao1* mutants. Scale bars are 10µm (A, C-E) and 25µm (B).

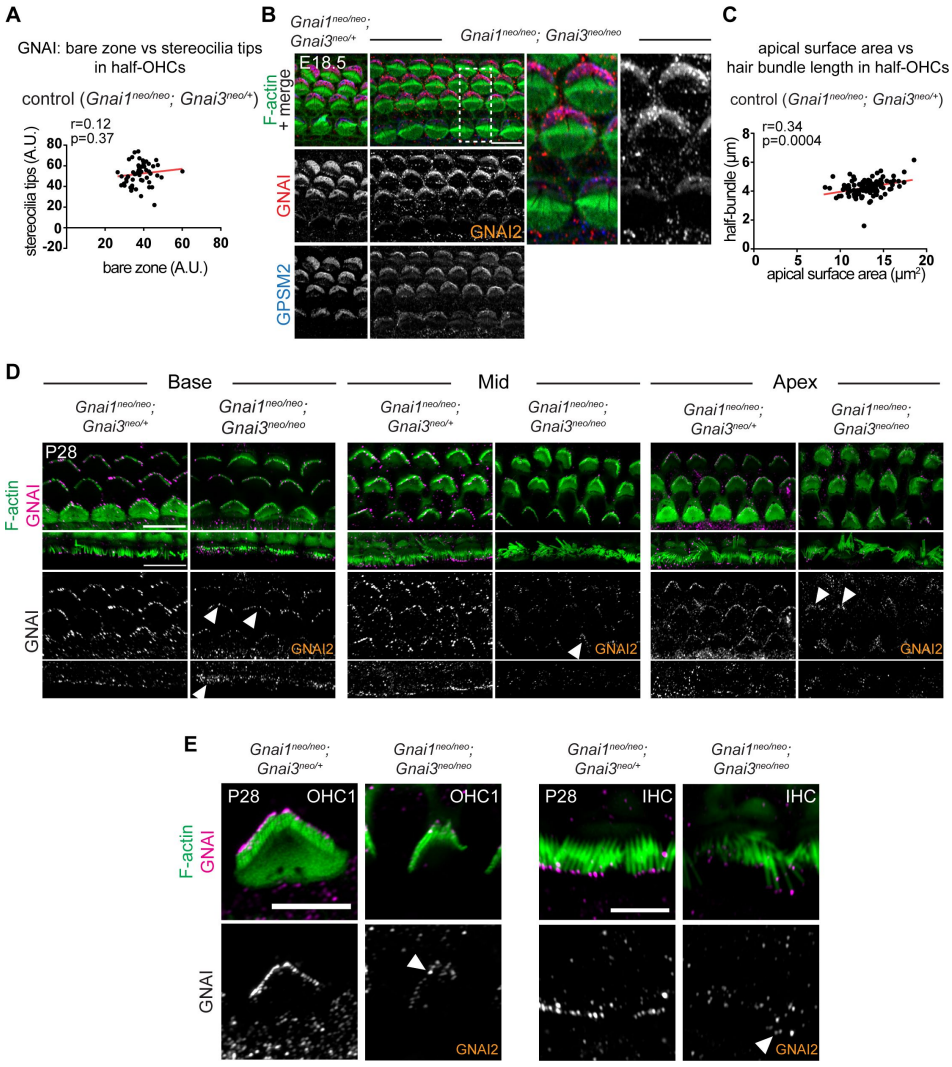

Figure 5 Supplement 1.

GNAI2 fully rescues loss of GNAI3 at embryonic stages and is still detected in low amounts at stereocilia tips in adult hair cells lacking GNAI3.

A) Control correlation plot for *Gnai1; Gnai3* double mutants in **Fig. 5C**. GNAI signal intensity at the bare zone and stereocilia tips in control half-HC at the P2 cochlear base. N=3 animals, n=40 OHC, Pearson correlation with best fit (red line). The graph shows relatively uniform GNAI enrichment in each sub-cellular compartment, unlike in *Gnai1; Gnai3* double mutants (**Fig. 5C**). **B)** GNAI (pt"GNAI2" antibody; see **Fig. 4**) and GPSM2 co-immunolabeling at the E18.5 5 cochlear base. As sole remaining GNAI, GNAI2 can still encompass the entire bare zone in *Gnai1; Gnai3* double mutants and no obvious hair bundle defects are observed, unlike at P0 (**Fig. 5A-B**). The boxed region is magnified to the right. **C)** Control correlation plot for *Gnai1; Gnai3* double mutants in **Fig. 5G**. The position of the basal body was used to determine the vertex (middle) of the hair bundle and to draw a radial line separating each OHC into two halves. The length of each hair bundle wing (y axis) is graphed in relation to the corresponding apical surface area (x axis) in the same half-OHC. The plot shows relatively uniform wing lengths and half apical areas in littermate controls, unlike in *Gnai1; Gnai3* double mutants (**Fig. 5G**). N=3 animals, n=52 OHC, Pearson correlation with best fit (red line). **D-E)** GNAI (pt"GNAI2" antibody; see **Fig. 4**) immunolabeling in P28 adults (maximum projections). As sole remaining GNAI, GNAI2 can still be detected at low levels at stereocilia tips in *Gnai1; Gnai3* double mutants at the cochlear base, mid and apex (arrowheads). E shows higher magnification views of a single OHC1 (left) and IHC (right) at the cochlear mid. A.U., arbitrary unit. Scale bars are 10µm (B, D) and 5 µm (E).

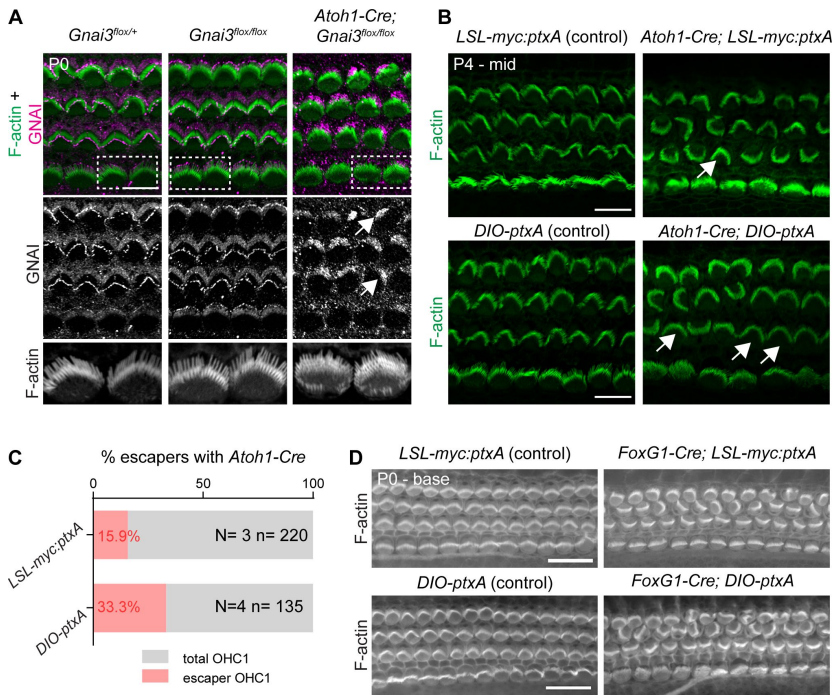

Figure 6 Supplement 1.

Validation of the *Gnai3*^{flox} and *DIO-ptxA* mouse strains.

A) GNAI (pt"GNAI2" antibody; see **Fig. 4**) immunolabeling at the P0 cochlear base. Note how in absence of Cre recombinase, *Gnai3*$^{flox/flox}$ HC have normal hair bundles and normal GNAI enrichment at the bare zone and stereocilia tips. In contrast, *Atoh1-Cre* produces incomplete GNAI enrichment (arrows; compare with **Fig. 4D**) and shortened stereocilia typical of constitutive *Gnai3* mutants. Boxed IHC regions are magnified below. **B-D)** Comparison of the two *ptxA* strains used in this study (see also **Fig. 2 Supp. 1C-D**). PtxA expression with the *Atoh1-Cre* driver produces comparable P4 apical HC defects in the *LSL-myc:ptxA* and *DIO- ptxA* strains (B). "Escaper" OHC1 that are not inverted in orientation (arrows) likely do not express Cre, or did not undergo recombination. **C)** When *Atoh1-Cre* induces ptxA expression in post-mitotic HC, the number of escaper OHC1 is higher in the *DIO-ptxA* strain. This is likely because *lox*-based genomic deletions (LSL) are favored over genomic inversions (DIO; see **Fig. 2 Supp. 1C-D**). **D)** In contrast to *Atoh1-Cre*, an earlier Cre driver (*FoxG1-Cre)* shows virtually no escapers in either ptxA strain. N and n indicate the number of animals and OHC1 analyzed, respectively. All *ptxA* samples in the study are heterozygotes (*R26*$^{LSL\text{-}myc:ptxA/+}$ or *R26*$^{DIO\text{-}ptxA/+}$), and controls are Cre-negative heterozygotes. Scale bars are 10µm (A, B), 20µm (D).

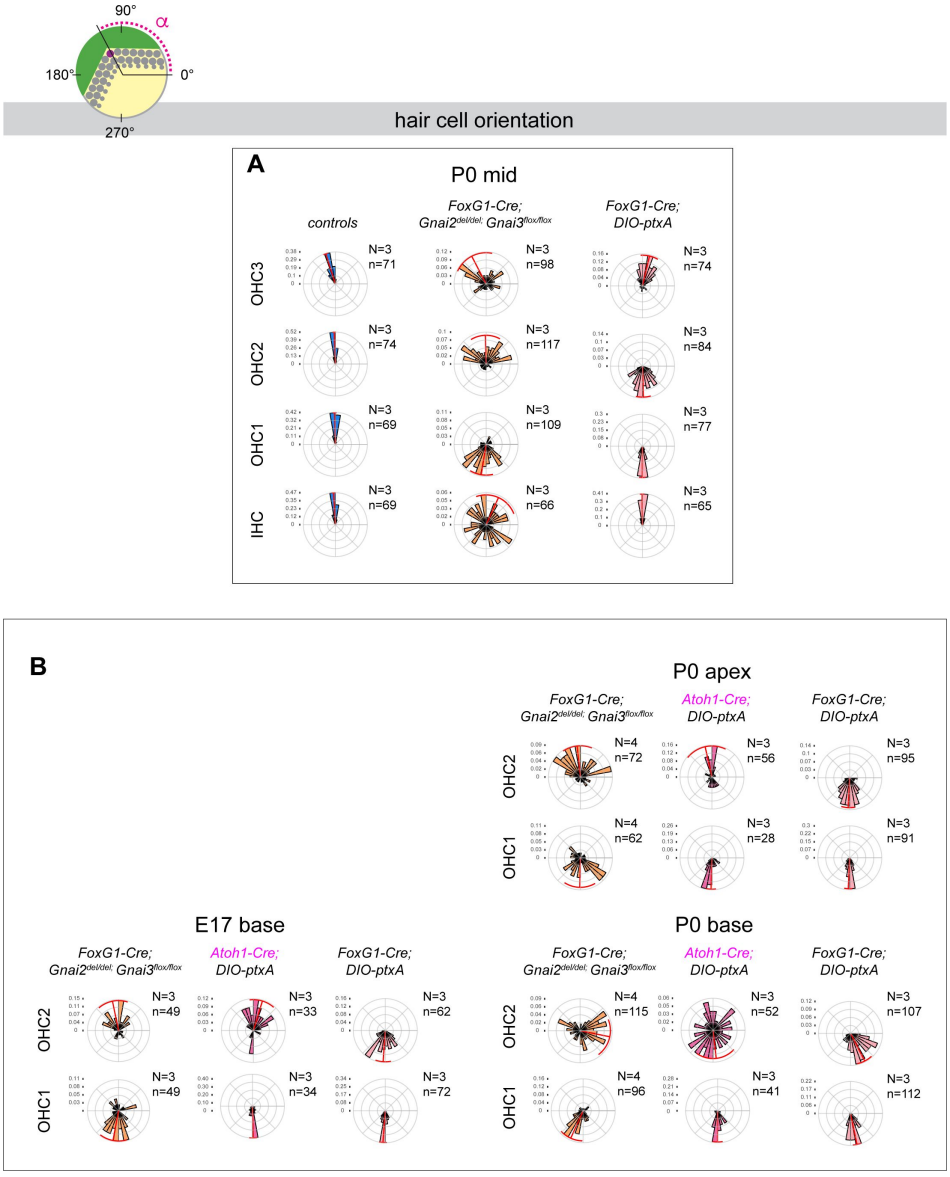

Figure 8 Supplement 1.

Loss of GNAI2 and GNAI3 recapitulates hair cell orientation defects observed in *ptxA* mutants.

A) P0 mid-cochlea histograms that complement P0 apex and P0 base histograms in **Fig. 8C-D**. **B)** Comparison of OHC1 and OHC2 orientation in *FoxG1-Cre; Gnai2*$^{del/del}$*; Gnai3*$^{flox/flox}$ (left diagrams; identical to **Fig. 8A, C**-D), *Atoh1-Cre; DIO-ptxA* (center diagrams) and *FoxG1- Cre; DIO-ptxA* mutants (right diagrams; identical to **Fig. 8A, C**-D) at the E17.5 base, P0 apex and P0 base. Post-mitotic Cre expression in *Atoh1-Cre* HC results in delayed *ptxA* expression and delayed inversion of OHC2 compared to earlier *FoxG1-Cre* expression in progenitor cells. This outcome is reminiscent of *Gnai2; Gnai3* mutants. At the E17.5 base and P0 apex (less mature), most OHC2s are inverted in the *FoxG1-Cre; DIO-ptxA* model only. At the P0 cochlear base (more mature), OHC2s are largely inverted in *Gnai2; Gnai3* mutants and in the *Atoh1-Cre; DIO-ptxA* model as well. Circular histograms show HC orientation (α) based on the position of the basal body (purple dot in top diagram) at the stage and cochlear position indicated. 0° is towards the cochlear base and 90° is lateral/abneural. HC represented have an eccentricity greater than 0.4 (E17.5) or 0.25 (P0) . Histograms show frequency distribution (10° bins) and red radial lines and arcs respectively indicate the circular mean and the circular mean deviation. n, HC number in N=3-4 animals. Littermate control histograms for *Atoh1-Cre; DIO-ptxA* mutants (B) can be found in **Fig. 8 Supp. 2F**.

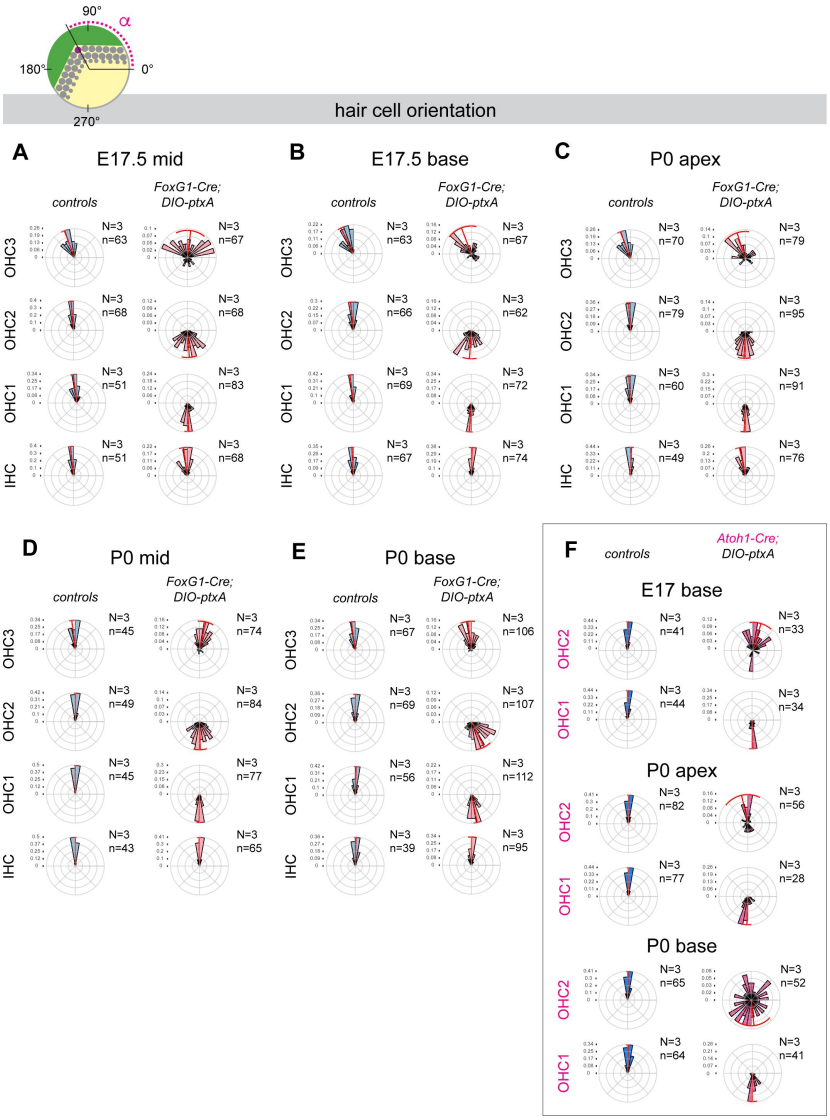

Figure 8 Supplement 2.

Littermate control histograms for *ptxA* mutants.

A-E) Histograms showing littermate controls for *FoxG1-Cre; DIO-ptxA* mutants in **Fig. 8** (A-C, E) and in **Fig. 8 Supp. 1A** (D; P0 mid), and littermate controls for *Atoh1-Cre; DIO-ptxA* mutants in **Fig. 8 Supp. 1B** (F). Note that mutant histograms are identical to **Fig. 8** or **Fig. 8 Supp. 1**. Circular histograms show HC orientation (α) based on the position of the basal body (purple dot in top diagram) at the stage and cochlear position indicated. 0° is towards the cochlear base and 90° is lateral/abneural. HC represented have an eccentricity above 0.4 at E17.5 and above 0.25 at P0. Histograms show frequency distribution (10° bins) and red radial lines and arcs respectively indicate the circular mean and the circular mean deviation. n, HC number in N=3-4 animals. Controls for *FoxG1-Cre; DIO-ptxA* and *Atoh1-Cre; DIO-ptxA* are Cre-negative *DIO- ptxA* heterozygotes. Detailed cohorts and results can be found in Source Data file.

Gene or model	Official name	Name in the study	MGI #	Reference	Allele description	Genetic background	Genetic background in the study	% surviving mutants at weaning age	
Gnai1	*Gnai1* ^{tm1Lbi}	*Gnai1* ^{neo}		Jiang et al, 2002 PMID: 36092739	neo cassette inserted in exon 3		129S1/SvImJ: C57BL/6J mix	*from het x het (expected 25%)* 16.4% (12 of 73 animals)	*from hom x het (expected 50%)* 45.8% (49 of 107 animals)
Gnai2	*Gnai2* ^{em1Btar}	*Gnai2* ^{del}		this study	CRISPR/Cas9 deletion of exons 2-3-4	C57BL/6J	C57BL/6J	9.9% (15 of 152 animals)	9.6% (5 of 52 animals)
							C57BL/6J: FVB/NJ mix	19.7% (12 of 61 animals)	46.7% (50 of 107 animals)
Gnai3	*Gnai3* ^{tm1Lbi}	*Gnai3* ^{neo}		Jiang et al, 2002 PMID: 36092739	part of intron 5 and exon 6 replaced with a neo cassette		129S1/SvImJ: C57BL/6J mix	30% (12 of 40 animals)	42% (63 of 150 animals)
		Gnai3 ^{flox}		this study	floxed exons 2-3	C57BL/6J	C57BL/6J		
Gnao1	*Gnao1* ^{tm1Lbi}	*Gnao1* ^{neo}	2152685	Jiang et al, 1998 PMID: 9501252	neo cassette inserted in exon 6	129S1/SvImJ	129S1/SvImJ	*from het x het (expected 25%)* 6.7% (3 animals out of 45)	
	Gnao1 $^{tm1c(EUCOMM)Hmgu}$	*Gnao1* ^{flox}	from 4456727	KOMP	floxed exon 3 - derived from Gnao1tm1a(EUCOMM)Hmgu via FLP-based removal of LacZneo cassette	C57BL/6N	C57BL/6N	*from Atoh1-Cre; het x het (expected 12.5% cKO)* 40% (10 *Atoh1-Cre; flox* hom of 25 animals)	*from Atoh1-Cre; hom x het (expected 25% cKO)* 30.7% (4 *Atoh1-Cre; flox* hom of 13 animals)
Gnai1; Gnai2	*Gnai1* ^{tm1Lbi} ; *Gnai2* ^{em1Btar}	*Gnai1* ^{neo} ; *Gnai2* ^{del}		Jiang et al, 2002 PMID: 36092739; this study			129S1/SvImJ: C57BL/6J:FVB/NJ mix	*from het; het x het (expected 6.25%)* 5,8% (7 of 121 animals)	*from hom; het x hom; het (expected 25% dKO)* 6.9% (2 of 29 animals)
Gnai1; Gnai3	*Gnai1* ^{tm1Lbi} ; *Gnai3* ^{tm1Lbi}	*Gnai1* ^{neo} ; *Gnai3* ^{neo}	5560183	Jiang et al, 2002 PMID: 36092739		129S1/SvImJ	129S1/SvImJ	*from hom; het x hom; het (expected 25% dKO)* 22.2% (20 of 90 animals)	*from hom; hom x hom; het (expected 50% dKO)* 43.2% (60 of 137 animals)
FoxG1-Cre; Gnai2; Gnai3		*Gnai2* ^{del} ; *Gnai3* ^{flox}		this study			129S1/SvImJ: C57BL/6J:FVB/NJ mix	*second generation crosses* 0% (0 out of 149 animals)	*first generation crosses* 0.3% (1 out of 333 animals)
ptxA	*Gt(ROSA)26Sor* $^{tm1(ptxA)Cgh}$	*LSL-ptxA:myc*	3776029	Regard et al, 2007 PMID: 17992256	*loxP-stop-loxP* cassette before *ptxA:myc*	C57BL/6:129SvJ			
	Gt(ROSA)26Sor $^{em1(ptxA)Btar}$	*LSL-myc:ptxA*	6163665	Tarchini et al, 2016 PMID: 27660326	*loxP-stop-loxP* cassette before *myc:ptxA*	C57BL/6J	C57BL/6J		
		DIO-ptxA		this study	double inverted *lox* sites flanking *ptxA*	C57BL/6J	C57BL/6J		
Atoh1-Cre	*Tg(Atoh1-cre)1Bfri*	*Atoh1-Cre*	3775845	Matei et al, 2005 PMID: 16145671	randomly inserted transgene with *Atoh1* enhancer	(C57BL/6 x CBA)F1	C57BL/6		
FoxG1-Cre	*Foxg* $^{1tm1(cre)Skm}$	*FoxG1-Cre*	1932522	Hebert et al, 2000 PMID: 10837119	Cre knock-in in the *FoxG1* gene	129P2/OlaHsd-Hprtb-m3	129S1/SvImJ: C57BL/6J mix		

Supplementary Table 1.

Mouse strain details.

Strain		Primer sequence	Bands size (bp)	
Gnao1 ^{flox}	forward	5' - TGGGTTTGATCCACAAGAGCGG - 3'		
	forward	5' - AGACGTGAAGCAGTACAAGC - 3'		
	reverse	5' - TCTCCTCAGTAGGGAAGATGGC - 3'		
			wt: 938; flox: 1119	wt: 387; flox: 421
Gnao1 ^{neo}	forward	5' - TGGTGACCCATTCTGACTTC - 3'		
	forward	5' - TCGCCTTCTATCGCCTTCTTGACG - 3'		
	reverse	5' - TTGGCAGAGAAAGCCCAAAG - 3'		
			wt: 836	neo: 461
Gnai1 ^{neo}	forward	5' - TCTAGGTGCTGGGGAATCTG - 3'		
	reverse	5' - GAGACGTGCTACTTCCATTTGTC - 3'		
	reverse	5' - TGAGCTTGTAGGCACAGAGG - 3'		
			wt: 1004	neo: 580
Gnai2 ^{del}	forward	5' -GCACCATCGTCAAGCAGATG - 3'		
	forward	5' - ATGGGTGGTTGTGAGCCATC - 3'		
	reverse	5' - GAGCTGGTATTCTCGTGAGC - 3'		
			wt: 728	wt: 1195; neo: 515
Gnai3 ^{neo}	forward	5' - CTTCTATCGCCTTCTTGACG - 3'		
	forward	5' -ACTCTGCTGACTTTGGCACC - 3'		
	reverse	5' - CTTTCATGCATTCGGTTCTG - 3'		
			wt: 762	neo: 450
Gnai3 ^{flox}	forward	5' - ATGAGGACGGCTATTCAGAG - 3'		
	reverse	5' - CATCCTACTTCACAAACTGC - 3'		XhoI digestion
			wt: 700; flox: 747	wt: 700; flox: 342 + 404
LSL-myc:ptxA	forward	5' - AAAGTCGCTCTGAGTTGTTAT - 3'		
	reverse	5' - GCGAAGAGTTTGTCCTCAACC - 3'		
	reverse	5' - GGAGCGGGAGAAATGGATATG - 3'		
			wt: 603	ptxA: 250
DIO-ptxA	forward	5' - GCACTTGCTCTCCCAAAGTC - 3'		
	reverse	5' - GGAGCGGGAGAAATGGATATG - 3'		
	reverse	5' - CGTCATTGACGTCAATAGGG - 3'		
			wt: 617	ptxA: 677
Atoh1-Cre	forward	5' - AGAGCGGCTGACAATAGAGG - 3'		
	reverse	5' - TTTCCATGAGTGAACGAACC - 3'		
			wt: no band	cre: 850
FoxG1-Cre	forward	5' - GCGACAAGAAGAACGGCAAG - 3'		
	forward	5' - GCAAGAACCTGATGGACATG - 3'		
	reverse	5' - AAGCACTTGTTGAGGGACAG - 3'		
	reverse	5' - TTTCCATGAGTGAACGAACC - 3'		
			wt: 202	cre: 381

Supplementary Table 2.

Genotyping strategies.

Bhonker Y. *et al.* (2016) **The GPSM2/LGN GoLoco motifs are essential for hearing** *Mamm Genome* **27**:29–46

Deans M. R (2013) **A balance of form and function: planar polarity and development of the vestibular maculae** *Semin Cell Dev Biol* **24**:490–8

Denman-Johnson K., Forge A (1999) **Establishment of hair bundle polarity and orientation in the developing vestibular system of the mouse** *J Neurocytol* **28**:821–35

Doherty D. *et al.* (2012) **GPSM2 mutations cause the brain malformations and hearing loss in Chudley-McCullough syndrome** *Am J Hum Genet* **90**:1088–93

Du Q., Stukenberg P. T., Macara I. G (2001) **A mammalian Partner of inscuteable binds NuMA and regulates mitotic spindle organization** *Nat Cell Biol* **3**:1069–75

Eisner D. A (2021) **Pseudoreplication in physiology: More means less** *J Gen Physiol* **153**

Etournay R., Lepelletier L., de Monvel Boutet, Michel J., Cayet V., Leibovici N., Weil M., Foucher D., Hardelin I., Petit J. P. (2010) **Cochlear outer hair cells undergo an apical circumference remodeling constrained by the hair bundle shape** *Development* **137**:1373–83

Ezan J. *et al.* (2013) **Primary cilium migration depends on G-protein signalling control of subapical cytoskeleton** *Nat Cell Biol* **15**:1107–15

Gilpatrick T., Lee I., Graham J. E., Raimondeau E., Bowen R., Heron A., Downs B., Sukumar S., Sedlazeck F. J., Timp W (2020) **Targeted nanopore sequencing with Cas9-guided adapter ligation** *Nat Biotechnol* **38**:433–438

Gohla A., Klement K., Piekorz R. P., Pexa K., vom Dahl S., Spicher K., Dreval V., Häussinger D., Birnbaumer L., Nürnberg B. (2007) **An obligatory requirement for the heterotrimeric G protein Gi3 in the antiautophagic action of insulin in the liver** *Proc Natl Acad Sci U S A* **104**:3003–8

Greene D. *et al.* (2023) **Genetic association analysis of 77,539 genomes reveals rare disease etiologies** *Nat Med*

Hebert J. M., McConnell S. K (2000) **Targeting of cre to the Foxg1 (BF-1) locus mediates loxP recombination in the telencephalon and other developing head structures** *Dev Biol* **222**:296–306

Jarysta A., Tarchini B (2021) **Multiple PDZ domain protein maintains patterning of the apical cytoskeleton in sensory hair cells** *Development* **148**

Jia S., Ratzan E. M., Goodrich E. J., Abrar R., Heiland L., Tarchini B., Deans M. R (2023) **The dark kinase STK32A regulates hair cell planar polarity opposite of EMX2 in the developing mouse inner ear** *Elife* **12**

Jiang M., Gold M. S., Boulay G., Spicher K., Peyton M., Brabet P., Srinivasan Y., Rudolph U., Ellison G., Birnbaumer L (1998) **Multiple neurological abnormalities in mice deficient in the G protein Go** *Proc Natl Acad Sci U S A* **95**:3269–74

Jiang M., Spicher K., Boulay G., Martin-Requero A., Dye C. A., Rudolph U., Birnbaumer L (2002) **Mouse gene knockout and knockin strategies in application to alpha subunits of Gi/Go family of G proteins** *Methods Enzymol* **344**:277–98

Jiang T., Kindt K., Wu D. K (2017) **Transcription factor Emx2 controls stereociliary bundle orientation of sensory hair cells** *Elife* **6**

Jones C., Roper V. C., Foucher I., Qian D., Banizs B., Petit C., Yoder B. K., Chen P (2008) **Ciliary proteins link basal body polarization to planar cell polarity regulation** *Nat Genet* **40**:69–77

Kindt K. S., Akturk A., Jarysta A., Day M., Beirl A., Flonard M., Tarchini B (2021) **EMX2-GPR156-Galphai reverses hair cell orientation in mechanosensory epithelia** *Nat Commun* **12**

Krey J. F., Chatterjee P., Halford J., Cunningham C. L., Perrin B. J., Barr-Gillespie P. G (2023) **Control of stereocilia length during development of hair bundles** *PLoS Biol* **21**

Locht C., Coutte L., Mielcarek N (2011) **The ins and outs of pertussis toxin** *FEBS J* **278**:4668–82

Low B. E., Hosur V., Lesbirel S., Wiles M. V (2022) **Efficient targeted transgenesis of large donor DNA into multiple mouse genetic backgrounds using bacteriophage Bxb1 integrase** *Sci Rep* **12**

Matei V., Pauley S., Kaing S., Rowitch D., Beisel K. W., Morris K., Feng F., Jones K., Lee J., Fritzsch B (2005) **Smaller inner ear sensory epithelia in Neurog 1 null mice are related to earlier hair cell cycle exit** *Dev Dyn* **234**:633–50

Mauriac S. A. *et al.* (2017) **Defective Gpsm2/Galphai3 signalling disrupts stereocilia development and growth cone actin dynamics in Chudley-McCullough syndrome** *Nat Commun* **8**

May-Simera H. L., Petralia R. S., Montcouquiol M., Wang Y. X., Szarama K. B., Liu Y., Lin W., Deans M. R., Pazour G. J., Kelley M. W (2015) **Ciliary proteins Bbs8 and Ift20 promote planar cell polarity in the cochlea** *Development* **142**:555–66

Mbiene J. P., Sans A (1986) **Differentiation and maturation of the sensory hair bundles in the fetal and postnatal vestibular receptors of the mouse: a scanning electron microscopy study** *J Comp Neurol* **254**:271–8

Montcouquiol M., Kelley M. W (2019) **Development and Patterning of the Cochlea: From Convergent Extension to Planar Polarity** *Cold Spring Harb Perspect Med*

Plummer N. W., Spicher K., Malphurs J., Akiyama H., Abramowitz J., Nürnberg B., Birnbaumer L (2012) **Development of the mammalian axial skeleton requires signaling through the Gα(i) subfamily of heterotrimeric G proteins** *Proc Natl Acad Sci U S A* **109**:21366–71

Qin W., Dion S. L., Kutny P. M., Zhang Y., Cheng A. W., Jillette N. L., Malhotra A., Geurts A. M., Chen Y. G., Wang H (2015) **Efficient CRISPR/Cas9-Mediated Genome Editing in Mice by Zygote Electroporation of Nuclease** *Genetics* **200**:423–30

Ramzan M., Bozan N., Seyhan S., Zafeer M. F., Ayral A., Duman D., Bademci G., Tekin M (2023) **Novel GPR156 variants confirm its role in moderate sensorineural hearing loss** *Sci Rep* **13**

Regard J. B., Kataoka H., Cano D. A., Camerer E., Yin L., Zheng Y. W., Scanlan T. S., Hebrok M., Coughlin S. R (2007) **Probing cell type-specific functions of Gi in vivo identifies GPCR regulators of insulin secretion** *J Clin Invest* **117**:4034–43

Schaefer M., Petronczki M., Dorner D., Forte M., Knoblich J. A (2001) **Heterotrimeric G proteins direct two modes of asymmetric cell division in the Drosophila nervous system** *Cell* **107**:183–94

Schaefer M., Shevchenko A., Shevchenko A., Knoblich J. A (2000) **A protein complex containing Inscuteable and the Galpha-binding protein Pins orients asymmetric cell divisions in Drosophila** *Curr Biol* **10**:353–62

Schnutgen F., Doerflinger N., Calleja C., Wendling O., Chambon P., Ghyselinck N. B (2003) **A directional strategy for monitoring Cre-mediated recombination at the cellular level in the mouse** *Nat Biotechnol* **21**:562–5

Siletti K., Tarchini B., Hudspeth A. J (2017) **Daple coordinates organ-wide and cell-intrinsic polarity to pattern inner-ear hair bundles** *Proc Natl Acad Sci U S A* **114**:E11170–E11179

Sipe C. W., Lu X (2011) **Kif3a regulates planar polarization of auditory hair cells through both ciliary and non-ciliary mechanisms** *Development* **138**:3441–9

Tadenev A. L. D., Akturk A., Devanney N., Mathur P. D., Clark A. M., Yang J., Tarchini B (2019) **GPSM2-GNAI Specifies the Tallest Stereocilia and Defines Hair Bundle Row Identity** *Curr Biol* **29**:921–934

Tarchini B (2021) **A Reversal in Hair Cell Orientation Organizes Both the Auditory and Vestibular Organs** *Front Neurosci* **15**

Tarchini B., Jolicoeur C., Cayouette M (2013) **A molecular blueprint at the apical surface establishes planar asymmetry in cochlear hair cells** *Dev Cell* **27**:88–102

Tarchini B., Lu X (2019) **New insights into regulation and function of planar polarity in the inner ear** *Neurosci Lett* **709**

Tarchini B., Tadenev A. L., Devanney N., Cayouette M (2016) **A link between planar polarity and staircase-like bundle architecture in hair cells** *Development* **143**:3926–3932

Tilney L. G., Tilney M. S., DeRosier D. J (1992) **Actin filaments, stereocilia, and hair cells: how cells count and measure** *Annu Rev Cell Biol* **8**:257–74

Tona Y., Wu D. K (2020) **Live imaging of hair bundle polarity acquisition demonstrates a critical timeline for transcription factor Emx2** *Elife* **9**

Walsh T. *et al.* (2010) **Whole exome sequencing and homozygosity mapping identify mutation in the cell polarity protein GPSM2 as the cause of nonsyndromic hearing loss DFNB82** *Am J Hum Genet* **87**:90–4

Watkins L. R., Orlandi C (2021) **In vitro profiling of orphan G protein coupled receptor (GPCR) constitutive activity** *Br J Pharmacol* **178**:2963–2975

Webb S. W., Grillet N., Andrade L. R., Xiong W., Swarthout L., Della Santina C. C., Kachar B., Muller U. (2011) **Regulation of PCDH15 function in mechanosensory hair cells by alternative splicing of the cytoplasmic domain** *Development* **138**:1607–17

Woodard G. E., Huang N. N., Cho H., Miki T., Tall G. G., Kehrl J. H (2010) **Ric-8A and Gi alpha recruit LGN, NuMA, and dynein to the cell cortex to help orient the mitotic spindle** *Mol Cell Biol* **30**:3519–30

Article and author information

Amandine Jarysta
The Jackson Laboratory, Bar Harbor, ME 04609, USA.
ORCID iD: 0000-0002-9519-3559

Abigail L.D. Tadenev
The Jackson Laboratory, Bar Harbor, ME 04609, USA.
ORCID iD: 0000-0003-0801-8267

Matthew Day
The Jackson Laboratory, Bar Harbor, ME 04609, USA.

Barry Krawchuk
The Jackson Laboratory, Bar Harbor, ME 04609, USA.

Benjamin E. Low
The Jackson Laboratory, Bar Harbor, ME 04609, USA.

Michael V. Wiles
The Jackson Laboratory, Bar Harbor, ME 04609, USA.

Basile Tarchini
The Jackson Laboratory, Bar Harbor, ME 04609, USA., Tufts University School of Medicine, Boston, MA 02111, USA
For correspondence: basile.tarchini@jax.org
ORCID iD: 0000-0003-2708-6273

Copyright

Editors

Reviewing Editor
Matthew Kelley
National Institute on Deafness and Other Communication Disorders, Bethesda, United States of America

Senior Editor
Didier Stainier
Max Planck Institute for Heart and Lung Research, Bad Nauheim, Germany

Reviewer #1 (Public Review):

A subclass of inhibitory heterotrimeric guanine nucleotide-binding protein subunits, GNAI, has been implicated in sensory hair cell formation, namely the establishment of hair bundle (stereocilia) orientation and staircase formation. However, the former role of hair bundle orientation has only been demonstrated in mutants expressing pertussis toxin, which blocks all GNAI subunits, but not in mutants with a single knockout of any of the Gnai genes, suggesting that there is a redundancy among various GNAI proteins in this role. Using various conditional mutants, the authors concluded that GNAI3 is the primary GNAI proteins required for hair bundle morphogenesis, whereas hair bundle orientation requires both GNAI2 and GNAI3.

Strength

Various compound mutants were generated to decipher the contribution of individual GNAI1, GNAI2, GNAI3 and GNAIO in the establishment of hair bundle orientation and morphogenesis. The study is thorough with detailed quantification of hair bundle orientation and morphogenesis, as well as auditory functions.

The revised manuscript has clarified the phenotypic differences raised between the Gnai2/3 double mutants and Ptx mutant phenotypes and resolved the weakness pointed out in the previous submission. These results further illustrate the dynamic requirement of Gnai/O in hair bundle establishment and is an important contribution to the field.

https://doi.org/10.7554/eLife.88186.2.sa1

Reviewer #2 (Public Review):

Jarysta and colleagues set out to define how similar GNAI/O family members contribute to the shape and orientation of stereocilia bundles on auditory hair cells. Previous work demonstrated that loss of particular GNAI proteins, or inhibition of GNAIs by pertussis toxin, caused several defects in hair bundle morphogenesis, but open questions remained which the authors sought to address. Some of these questions include whether all phenotypes resulting from expression of pertussis toxin stemmed from GNAI inhibition; which GNAI family members are most critical for directing bundle development; whether GNAI proteins are needed for basal body movements that contribute to bundle patterning. These questions are important for understanding how tissue is patterned in response to planar cell polarity cues.

To address questions related to the GNAI family in auditory hair cell development, the authors assembled an impressive and nearly comprehensive collection of mouse models. This approach allowed for each Gnai and Gnao gene to be knocked out individually or in combination with each other. Notably, a new floxed allele was generated for Gnai3 because loss of this gene in combination with Gnai2 deletion was known to be embryonic lethal. Besides these lines, a new knockin mouse was made to conditionally express untagged pertussis toxin following cre induction from a strong promoter. The breadth and complexity involved in generating and collecting these strains makes this study unique, and likely the authoritative last word on which GNAI proteins are needed for which aspect of auditory hair bundle development.

Appropriate methods were employed by the authors to characterize auditory hair bundle morphology in each mouse line. Conclusions were carefully drawn from the data and largely based on excellent quantitative analysis. The main conclusions are that GNAI3 has the largest effect on hair bundle development. GNAI2 can compensate for GNAI3 loss in early development but incompletely in late development. The Gnai2 Gnai3 double mutant

recapitulates nearly all the phenotypic effects associated with pertussis toxin expression and also reveals a role for GNAIs in early movement of the basal body. This comprehensive study builds on earlier reports, both uncovering new functions and putting previously putative functions on solid ground.

https://doi.org/10.7554/eLife.88186.2.sa0

Author Response

The following is the authors' response to the current reviews.

> ***Recommendations for the authors:***
>
> ***Reviewer #1 (Recommendations For The Authors):***
>
> *Hats off to the authors for taking time to decipher the seemingly subtle but important differences between the Gnai2/3 double mutant and Ptx mutant phenotypes. These results further illustrate the dynamic requirement of Gnai/0 in hair bundle establishment. I have some minor suggestions for the authors to consider and it is up to the authors to decide whether to incorporate them:*

We decided to make the current (revised) version the version of record, and we explain why below. Please include these comments in the review+rebuttal material.

> *(1) The abstract could be modified to reflect the revised interpretations of the results.*

Response: the abstract is high-level and the changes in interpretation in the revised manuscript do not modify the message there. Briefly, the abstract only states that Gnai2; Gnai3 double mutants recapitulate two defects previously only observed with pertussis toxin. There is no claim about the timing or dose of GNAI proteins involved.

> *(2) The three rows of OHCs are like a different beast from each other. Mireille Montcouquiol's lab has demonstrated that there is a differential requirement for Gnai3 in hair bundle orientation among the three rows of OHCs. The results described in this manuscript support this notion as well.*

To clarify, Gnai3 inactivation does not affect OHC orientation. Only pertussis toxin, and in this work Gnai2; Gnai3 double mutants, do. The Montcouquiol lab showed different degree of OHC1, OHC2 and OHC3 misorientation upon use of pertussis toxin in vitro using cochlear explants (Ezan et al 2013). We showed the same thing in vivo using transgenic models (Tarchini et al 2013; Tarchini et al 2016). The different OHC responses by row and corresponding citations are mentioned in several locations in the manuscript, including first on line 112 in the Introduction and in Fig. 1C in a graphical summary.

> *(3) I wonder if "compensate" or "redundancy" may be a better term to use than "rescue" in the Discussion and figure.*

Use of "rescue" in the Discussion is line 603 and 604. We think that "rescue" is appropriate to refer to the ability of GNAI2 to compensate for the loss of GNAI1 and GNAI3 in mutant context. We would argue that these different wordings are largely interchangeable and do not change the message.

Author Response

The following is the authors' response to the original reviews.

We really appreciate the time the reviewers spent reading and commenting on the original manuscript. Although they were positive already, we decided to spend some time to address the main comments with new experiments as thoroughly as possible in a new manuscript version. We also heavily edited some sections accordingly.: 1) we delayed pertussis toxin activation in hair cells with Atoh1-Cre to show that the resulting misorientation phenotype is delayed compared to FoxG1-Cre results, as also seen in Gnai2; Gnai3 double mutants. It follows that Gnai2; Gnai3 and pertussis mutants do share a similar misorientation profile, and that GNAI proteins are required to normally reverse OHC1-2 (from medial to lateral), but also to maintain the lateral orientation, at least transiently. 2) We experimentally verified that one of our GNAI antibodies can indeed detect GNAI1, and consequently that absence of signal in Gnai2; Gnai3 double mutants is evidence that GNAI1 is not involved in apical hair cell polarization. We believe these changes strengthen the manuscript and its conclusions.

> ***Reviewer #1 (Public Review):***
>
> *A subclass of inhibitory heterotrimeric guanine nucleotide-binding protein subunits, GNAI, has been implicated in sensory hair cell formation, namely the establishment of hair bundle (stereocilia) orientation and staircase formation. However, the former role of hair bundle orientation has only been demonstrated in mutants expressing pertussis toxin, which blocks all GNAI subunits, but not in mutants with a single knockout of any of the Gnai genes, suggesting that there is a redundancy among various GNAI proteins in this role. Using various conditional mutants, the authors concluded that GNAI3 is the primary GNAI proteins required for hair bundle morphogenesis, whereas hair bundle orientation requires both GNAI2 and GNAI3.*
>
> *Strength*
>
> *Various compound mutants were generated to decipher the contribution of individual GNAI1, GNAI2, GNAI3 and GNAIO in the establishment of hair bundle orientation and morphogenesis. The study is thorough with detailed quantification of hair bundle orientation and morphogenesis, as well as auditory functions.*
>
> *Weakness*
>
> *While the hair bundle orientation phenotype in the Foxg1-cre; Gnai2-/-; Gnai3 lox/lox (double mutants) appear more severe than those observed in Ptx cKO mutants, it may be an oversimplification to attribute the differences to more GNAI function in the Ptx cko mutants. The phenotypes between the double mutants and Ptx cko mutants appear qualitatively different. For example, assuming the milder phenotypes in the Ptx cKO is due to incomplete loss of GNAI function, one would expect the Ptx phenotype would be reproducible by some combination of compound mutants among various Gnai genes. Such information was not provided. Furthermore, of all the double mutant specimens analyzed for hair bundle orientation (Fig. 8), the hair bundle/kinocilium position started out normally in the lateral quadrant at E17.5 but failed to be maintained by P0. This does not appear to be the case for Ptx cKO, in which all affected hair cells showed inverted orientation by E17.5. It is not clear whether this is the end-stage of bundle orientation in Ptx cKO, and the kinocilium position started out normal, similar to the double mutants before the age of analysis at E17.5. Understanding these differences may reveal specific requirements of individual GNAI subunits or other factors are being affected in the Ptx mutants.*

This criticism was very useful and prompted new experiments as well as a change in data presentation and a fundamental rewrite regarding hair cell orientation. These changes are detailed below. Of note, however, please let us clarify that the original manuscript did show that the ptxA orientation phenotype is reproduced to some extent in Gnai2; Gnai3 double mutants (previously Fig. 8 and corresponding text line 505). We showed that OHC1-2 are also inverted in the double mutant, although at a later differentiation stage. We recognize that similarities in hair cell misorientation between ptxA and Gnai2; Gnai3 DKO were not explained and discussed well enough. This part of the manuscript has been re-worked extensively, and we hope that along with new results, comparisons between mutant models are easier to follow and understand. We notably fully adopted the idea that there are qualitative differences between ptxA and Gnai2; Gnai3 mutants, and not only a difference in the remaining "dose" of GNAI activity.

> ***Recommendations for the authors:***
>
> ***Reviewer #1 (Recommendations For The Authors):***
>
> *Comments related to clarification of the weakness:*
>
> *(1) In general, hair bundle orientation in the double mutants is established in the lateral quadrant of the cochlea before being inverted (Fig. 8). These results are intriguing because the lateral orientation is the correct position for these hair bundles normally and Gnai proteins are thought to be required to get the kinocilium to the lateral position. This process appears to proceed normally in the double mutants but the kinocilium reverted to the medial default position over time, which suggests that Gnai2 and Gnai3 are only required for the maintenance and not the establishment of the kinocilium in the lateral position. Is this phenotype qualitatively similar in the Ptx cKO?*

We addressed these issues with two types of modifications to the data:

(1) We modified the eccentricity threshold used at E17.5 in Fig. 8 (orientation) to be more stringent, using 0.4 (instead of 0.25 previously) in both controls and mutants. This means that we now only graph the orientation of cells where eccentricity is more marked. The rationale is that at early stages, it is challenging to distinguish immature vs defective near-symmetrical cells. We kept a threshold of 0.25 at P0 when the hair cell apical surface is larger and better differentiated (Fig. 8C-D). Importantly, the dataset remains rigorously identical. This change usefully highlights that a large proportion of OHC1 is in fact inverted (oriented medially) at E17.5 in Gnai2; Gnai3 double mutants at the cochlear mid, as also seen in the ptxA model at the same stage and position (see new Fig. 8A). At the E17.5 base (Fig. 8B), a slightly more mature position, the outcome is unchanged (the majority of OHC1 are inverted using either a 0.25 or 0.4 threshold in double mutants and in ptxA).

Interestingly however, the orientation trend is unchanged for OHC2: OHC2 remain oriented largely laterally (i.e. normally) at the E17.5 mid and base in Gnai2; Gnai3 double mutants even with a raised eccentricity thresholds, whereas by contrast OHC2 in ptxA are inverted at these stage and positions. In the double mutant, OHC2 only become inverted at the P0 base (Fig. 8D). This suggests that there are similarities (OHC1) but also differences (OHC2s) between the two mouse models, and that double mutants show a delay in adopting an inverted orientation compared to ptxA. Of note, OHC2 have been shown to differentiate later than OHC1 (for example, Anniko 1983 PMID:6869851).

(2) To directly test the idea that the misorientation phenotype (inverted OHC1-2) is comparable between the two models but delayed in Gnai2; Gnai3 mutants, we performed a new experiment and added new results in the manuscript. We delayed ptxA action by using Atoh1-Cre (postmitotic hair cells) instead of FoxG1-Cre (otic progenitors). Remarkably, this

produced a pattern of OHC1-2 misorientation more similar to Gnai2; Gnai3 mutants: at the E17.5 base and P0 apex, OHC2 were still largely oriented laterally (normally) in Atoh1-Cre; ptxA as in Gnai2; Gnai3 mutants whereas at the P0 base a large proportion of OHC2 were inverted (Fig. 8 Supp 1B). OHC1 were inverted at all stages and positions in the Atoh1-Cre as in the FoxG1-Cre; ptxA model. For Atoh1-Cre; ptxA, we only illustrated OHC1 and OHC2 and did not add E17.5 mid or P0 mid results because other cell types and stage/positions did not provide additional insight. In addition, we are well aware that the full FoxG1-Cre; ptxA and Gnai2; Gnai3 results for 4 cells types (IHC, OHC1-3) and 5 stages/positions is already a lot of data for cell orientation.

These results suggest that:

(a) The normal reversal of OHC1-2 to adopt a lateral orientation needs to be maintained, at least transiently, and that maintenance also relies on GNAI/O (Results starting line 529. Disussion line 621).

(b) ptxA is more severe than Gnai2; Gnai3 when it comes to OHC1-2 orientation (Figure 9, role b). Oppositely, Gnai2; Gnai3 is obviously more severe when it comes to symmetry-breaking (Fig. 9, role a) and hair bundle morphogenesis (Fig. 9, c). It follows that the two early GNAI/O activities are qualitatively different and not just based on dose. This is essentially what this Reviewer correctly pointed out, and we have fully edited both Results and Discussion accordingly. We now speculate that the difference may lie in the identity of the necessary GNAI/O protein for each role. Any GNAI/O proteins acting as a switch downstream of the GPR156 receptor may relay orientation information (Fig. 9, role b), making ptxA a particularly effective disruption strategy since it downregulates all GNAI/O proteins. In contrast, symmetry-breaking may rely more specifically on GNAI2 and GNAI3, and ptxA is not expected to achieve a loss-of-function of GNAI2 and GNAI3 as extensive as a double targeted genetic inactivation of the corresponding genes. Please see new Results starting line 526 and Discussion starting line 603. We consequently abandoned the notion that increased doses of GNAI/O is required for each role, and we also clarify that symmetry-breaking (a) and orientation (b) occur at the same time (Fig. 9).

> *(2) P0 may not be late enough a stage to access phenotype maturity in the double mutants. For example, it is not clear from the basal PO results whether the IHC will acquire an inverted phenotype or just misorientation in the lateral side.*

For context, the OHC1-2 misorientation pattern in the ptxA model at P0 does represent the end stage, as the same pattern is observed in adults (illustrated in Fig. 2A). In addition, OHC1-2 that express ptxA are inverted as soon as they break planar symmetry, and this was established at E16.5 in a previous publication where ptxA and Gpr156 misorientation patterns were compared and shown to be identical (Kindt et al., 2021 Supp. fig. 5C-D). However, we clearly failed to mention these important results in the original manuscript. We now cite Figure 2 for adult defects (line 522), and provide a citation for OHC1-2 inversion being observed from earliest stage of hair cell differentiation (Kindt et al., 2021) (line 519).

The vast majority of Gnai2; Gnai3 double mutants die before weaning but the single specimen we managed to collect at P21 also showed inverted OHC1-2 (representative example in Fig. 2A). Again, we previously failed to point out this important result. We now do so line 214 and 555. This is another evidence that OHC1-2 misorientation is in fact similar in the ptxA and Gnai2; Gnai3 models (but milder and delayed in the latter).

When it comes to IHCs and OHC3s however, the situation is less clear. These cell types are mildly misoriented in ptxA and Gpr156 mutants, but IHCs in particular appear severely misoriented in Gnai2; Gnai3 mutants based on the position of the basal body (Fig. 8). However, very dysmorphic hair bundles can pull on the basal body via the kinocilium and affect its position, which obscures hair cell orientation inferred from the basal body and

subsequent interpretations. We do not delve on IHC and OHC3 and their orientation in Gnai2; Gnai3 mutants in the revision since we do not observe similar orientation defects in a different mouse model and lack sufficient adult data.

> *Suggestions to improve upon the manuscript for readers:*
>
> *(1) Line 294, indicate on the figure the staining in bare zone and tips of stereocilia on row 1.*

Pertains to Figure 4. In A, we now point out the bare zone and stereocilia tips with arrow and arrowheads, respectively (as in other figures).

> *(2) Fig.8 schematic diagram, the labels of the line and 90o side by side is misleading.*

We added black ticks for 0, 90, 180, 270 degree references. In contrast, the hair cell angle represented was switched to magenta.

> *(3) Fig. 7 legend, redundancy towards the end of the paragraph.*

Thank you for catching this issue. A large portion of the legend was indeed accidentally repeated and is now deleted.

> *(4) Line 490-493, Another plausible explanation is that other factors besides Gnai2 and Gnai3 are involved in breaking symmetry during bundle establishment.*

We now acknowledge that other proteins besides GNAI/O may be involved (Discussion line 614). That said, the notion that we do not achieve sufficient and/or early enough GNAI loss is supported for example by the Beer-Hammer 2018 study where no defects in symmetry-breaking or orientation were reported in their Gnai2 flox/flox; Gnai3 flox/flox model (Discussion new Line 637).

> *(5) Line 518, the base were largely inverted (Figure 8B). Should Fig 8A be cited instead of 8B?*

Fig. 8B has graphs for the E17.5 cochlear base where OHC1-2 are inverted in both ptxA and Gnai2;3 DKO models. Fig. 8A has graphs of the E17.5 cochlear mid (less differentiated hair cells) where an inversion was not obvious previously, but is now clear although only partial in Gnai2; Gnai3 DKO (see above; raised eccentricity threshold). In the context of the previous text, this citation was thus correct. However, this section has been heavily modified to better compare Gnai2; Gnai3 DKO and ptxA and is hopefully less confusing in the revised version.

> ***Reviewer #2 (Public Review):***
>
> *Jarysta and colleagues set out to define how similar GNAI/O family members contribute to the shape and orientation of stereocilia bundles on auditory hair cells. Previous work demonstrated that loss of particular GNAI proteins, or inhibition of GNAIs by pertussis toxin, caused several defects in hair bundle morphogenesis, but open questions remained which the authors sought to address. Some of these questions include whether all phenotypes resulting from expression of pertussis toxin stemmed from GNAI inhibition; which GNAI family members are most critical for directing bundle development; whether GNAI proteins are needed for basal body movements that contribute to bundle patterning. These questions are important for understanding how tissue is patterned in response to planar cell polarity cues.*

> *To address questions related to the GNAI family in auditory hair cell development, the authors assembled an impressive and nearly comprehensive collection of mouse models. This approach allowed for each Gnai and Gnao gene to be knocked out individually or in combination with each other. Notably, a new floxed allele was generated for Gnai3 because loss of this gene in combination with Gnai2 deletion was known to be embryonic lethal. Besides these lines, a new knockin mouse was made to conditionally express untagged pertussis toxin following cre induction from a strong promoter. The breadth and complexity involved in generating and collecting these strains makes this study unique, and likely the authoritative last word on which GNAI proteins are needed for which aspect of auditory hair bundle development.*
>
> *Appropriate methods were employed by the authors to characterize auditory hair bundle morphology in each mouse line. Conclusions were carefully drawn from the data and largely based on excellent quantitative analysis. The main conclusions are that GNAI3 has the largest effect on hair bundle development. GNAI2 can compensate for GNAI3 loss in early development but incompletely in late development. The Gnai2 Gnai3 double mutant recapitulates nearly all the phenotypic effects associated with pertussis toxin expression and also reveals a role for GNAIs in early movement of the basal body. Although these results are not entirely unexpected based on earlier reports, the current results both uncover new functions and put putative functions on more solid ground.*
>
> *Based on this study, loss of GNAI1 and GNAO show a slight shortening of the tallest row of stereocilia but no other significant changes to bundle shape. Antibody staining shows no change in GNAI localization in the Gnai1 knockout, suggesting that little to no protein is found in hair cells. One caveat to this interpretation is that the antibody, while proposed to cross-react with GNAI1, is not clearly shown to immunolabel GNAI1. More than anything, this reservation mostly serves to illustrate how challenging it is to nail down every last detail. In turn, the comprehensive nature of the current study seems all the more impressive.*

(1) The original manuscript quantified stereocilia properties in Gnai1 and Gnai2 single mutants, and in Gnai1; Gnai2 double mutants using non-parametric t-tests (Mann-Whitney) for comparisons. This approach indeed suggested subtle reduction in row 1 height in IHCs in all 3 mutants. We did not quantify stereocilia features in Gnao1 mutants but could not observe defects (new Fig. 2 Supp. 1E-F). In fact, we could not observe defects in Gnai1 and Gnai2 single mutants, and in Gnai1; Gnai2 double mutants either. For this reason we have been ambivalent about reporting defects for Gnai1 and Gnai2 single and Gnai1; Gnai2 double mutants.

In the revision, we applied a nested (hierarchical) t-test to avoid pseudo-replication (Eisner 2021; PMID: 33464305; https://pubmed.ncbi.nlm.nih.gov/33464305/). In our data, the nested t-tests structure measurements by animal instead of having all stereocilia or other cell measurements treated as independent values. This more stringent approach no longer finds row 1 height reduction significant in single Gnai1 or Gnai2 mutants, or in Gnai1; Gnai2 double mutants. We modified the text accordingly in Results and Discussion. Nested t-tests were applied uniformly across the manuscript and, besides IHC measurements in Fig. 2, now also apply to bare zone surface area in Fig. 6 and eccentricity in Fig. 7. For these experiments in contrast, previous conclusions are not changed. We think that this more careful statistical treatment is a closer representation of the data in term of the conclusions we can safely make.

(2) The reviewer's criticism about antibody specificity is accurate and fair, and is fully addressed in the revised manuscript. First, we provide a phylogeny cartoon as Figure 1A to compare the GNAI/O proteins and highlight how closely related they are in sequence. To validate the assumption that our approach would detect GNAI1 if it were present in hair cells,

we took a new dual experimental approach in the revision. First, we electroporated Gnai1, Gnai2 and Gnai3 expression constructs in the E13.5 inner ear and tested whether the two GNAI antibodies used in the study can detect ectopic GNAI1 in Kolliker organ. This revealed that “ptGNAI2” detects GNAI1 very well (in addition to GNAI2), but that “scbtGNAI3” does not detect GNAI1 efficiently (although it does detect GNAI3 very well). To verify in vivo that “ptGNAI2” can detect endogenous GNAI1, we immunolabeled the gallbladder epithelium in Gnai1 mutants and littermate controls using the “ptGNAI2” antibody. Based on IMPC consortium data* about the Gnai1 LacZ mouse strain, Gnai1 is specifically expressed in the adult gallbladder. We could verify that signals detected in the Gnai1 mutants were visually reduced in comparison to littermate controls. We now added this validation step in Results line 309 and the data in Fig. 4 Supp. 1A-B).

*https://www.mousephenotype.org/data/genes/MGI:95771

> ***Reviewer #2 (Recommendations For The Authors):***
>
> *Minor comments that may marginally improve clarity.*
>
> *Abstract line 24: delete "nor polarized" because polarization cannot be assessed since the protein is undetectable.*

This is a fair point, now deleted.

> *Consider revising: Lines 80-82; 188-202 (the order in which the mutants were presented was hard to follow for me); 239-240.*

Lines 80-82: Used to read as "Ptx recapitulates severe stereocilia stunting and immature-looking hair bundles observed when GPSM2 or both GNAI2 and GNAI3 are inactivated."

Line 88: Was now changed to "Ptx provokes immature-looking hair bundles with severely stunted stereocilia, mimicking defects in Gpsm2 mutants and Gnai2; Gnai3 double mutants".

Lines 188-202: This was the first paragraph describing adult stereocilia defects in the different Gnai/o mouse strains. We completely rewrote the entire section to reflect the order in which the strains appear in Figure 2, hopefully making the text easier to follow because it better matches panels in Fig. 2 . We also made several other modifications to streamline comparisons and better introduce the orientation defects that are later detailed at neonate stages.

Lines 239-240: Used to read "GNAI2 makes a clear contribution since stereocilia defects increase in severity when GNAI loss extends from GNAI3 to both GNAI2 and GNAI3".

Line 247: Was now changed for "GNAI2 makes a clear contribution since Gnai3neo stereocilia defects dramatically increase in severity when GNAI2 is absent as well in Gnai2; Gnai3 double mutants."

> *Line 164: hardwired is unclear. Conserved?*

We modified this sentence as follows: Line 171: "We reasoned that apical HC development is probably highly constrained and less likely to be influenced by genetic heterogeneity compared to susceptibility to disease, for example."

> *Line 299: It is not clear why GNAI1 is a better target than GNAI3. This phrase is repeated in line 303, I suspect inadvertently. Is there evidence that this antibody detects GNAI1, perhaps in another tissue? Line 308: GNAI1 may also not be detected by this antibody.*

Please see point 2 above. We removed these hypothetical statements entirely and we instead now experimentally show that one of the two commercial antibodies used can readily detect GNAI1 (yet does not detect signal in hair cells when GNAI2 and GNAI3 are absent in Fig. 4F).